Inorganic Chemistry
Article

Inorg. Chem. **2011**, *50*, 525–538 **525**
DOI: 10.1021/ic101384p

Chemistry and Catalytic Activity of Molybdenum(VI)-Pyrazolylpyridine Complexes in Olefin Epoxidation. Crystal Structures of Monomeric Dioxo, Dioxo-μ-oxo, and Oxodiperoxo Derivatives

Ana C. Coelho,[†] Mariela Nolasco,[†] Salete S. Balula,[†,‡] Margarida M. Antunes,[†] Cláudia C. L. Pereira,[†,§] Filipe A. Almeida Paz,[†] Anabela A. Valente,[†] Martyn Pillinger,[†] Paulo Ribeiro-Claro,[†] Jacek Klinowski,[∥] and Isabel S. Gonçalves*[,†]

[†]*Department of Chemistry, CICECO, University of Aveiro, 3810-193 Aveiro, Portugal,* [‡]*REQUIMTE/Department of Chemistry and Biochemistry, Faculty of Science, University of Porto, 4169-007 Porto, Portugal,* [§]*Unit of Chemical and Radiopharmaceutical Sciences (UCRS), Nuclear and Technological Institute, Estrada Nacional 10, 2686-953 Sacavém, Portugal, and* [∥]*Department of Chemistry, University of Cambridge, Lensfield Road, Cambridge CB2 1EW, U.K.*

Received July 12, 2010

The dioxomolybdenum(VI) complexes $[MoO_2Cl_2(PzPy)]$ (**1**) and $[MoO_2(OSiPh_3)_2(PzPy)]$ (**5**) (PzPy = 2-[3(5)-pyrazolyl]pyridine) were synthesized and characterized by vibrational spectroscopy, with assignments being supported by DFT calculations. Complex **5** was additionally characterized by single crystal X-ray diffraction. Recrystallization of **1** under different conditions originated crystal structures containing either the mononuclear $[MoO_2Cl_2(PzPy)]$ complex co-crystallized with 2-[3(5)-pyrazolyl]pyridinium chloride, binuclear $[Mo_2O_4(\mu_2\text{-}O)Cl_2\text{-}(PzPy)_2]$ complexes, or the oxodiperoxomolybdenum(VI) complex $[MoO(O_2)_2Cl(PzPyH)]$, in which a 2-[3(5)-pyrazolyl]pyridinium cation weakly interacts with the Mo^{VI} center via a pyrazolyl N-atom. The crystal packing in the different structures is mediated by a variety of supramolecular interactions: hydrogen bonding involving the pyridinium and/or pyrazolyl N−H groups, weak CH···O and CH···π contacts, and strong $\pi-\pi$ stacking. Complexes **1** and **5** are moderately active catalysts for the epoxidation of *cis*-cyclooctene at 55 °C using *tert*-butylhydroperoxide as oxidant, giving 1,2-epoxycyclooctane as the only reaction product. Insoluble materials were recovered at the end of the first catalytic runs and characterized by IR spectroscopy, elemental analysis, scanning electron microscopy (SEM)-energy dispersive spectroscopy (EDS), and powder X-ray diffraction. For complex **5** the loss of the triphenylsiloxy ligands during the catalytic run resulted in the formation of a tetranuclear complex, $[Mo_4O_8(\mu_2\text{-}O)_4(PzPy)_4]$. The recovered solids could be used as efficient heterogeneous catalysts for the epoxidation of cyclooctene, showing no loss of catalytic performance between successive catalytic runs.

Introduction

Among the various oxyhalides of molybdenum, dichlorodioxomolybdenum(VI) (MoO_2Cl_2) has received much attention especially as a catalyst for organic transformations.[1,2] Treatment of MoO_2Cl_2 with oxygen or nitrogen donor ligands such as tetrahydrofuran (THF), *N*,*N*-dialkylamides, phosphine oxides, 3,5-dimethylpyrazole, 2,2′-bipyridine and 1,10-phenanthroline gives adducts with the general formulas $[MoO_2Cl_2(L)_2]$ and $[MoO_2Cl_2L]$ for monodentate and bidentate ligands, respectively.[3,4] With a few exceptions, these monomeric complexes adopt a *cis*-oxo, *trans*-Cl, *cis*-L configuration at the metal center and a distorted octahedral coordination geometry.[5] Depending on the choice of ligand (L), the complexes exhibit moderate to excellent catalytic performance for the liquid-phase epoxidation of olefins using *tert*-butylhydroperoxide (TBHP) as the mono-oxygen source.[4,6] Concerning the reaction mechanism, it is generally proposed that the hydroperoxide (a Lewis base) coordinates to the metal center (a Lewis acid) by the terminal oxygen atom, followed by oxygen atom transfer from the intermediate oxidizing species to the olefin, producing the epoxide and concomitant elimination of *tert*-butyl alcohol. The catalytic activity of a given complex is sensitive to the donor/acceptor

*To whom correspondence should be addressed. Fax: +351 234 420634. E-mail: igoncalves@ua.pt.

(1) For a recent review see: Jeyakumar, K.; Chand, D. K. *J. Chem. Sci.* **2009**, *121*, 111–123.

(2) (a) de Noronha, R. G.; Fernandes, A. C.; Romão, C. C. *Tetrahedron Lett.* **2009**, *50*, 1407–1410. (b) de Noronha, R. G.; Costa, P. J.; Romão, C. C.; Calhorda, M. J.; Fernandes, A. C. *Organometallics* **2009**, *28*, 6206–6212. (c) Calhorda, M. J.; Costa, P. J. *Dalton Trans.* **2009**, 8155–8161.

(3) For a recent review see: Abramenko, V. L.; Sergienko, V. S. *Russ. J. Inorg. Chem.* **2009**, *54*, 2031–2053.

Published on Web 12/09/2010

ability of the ligand, and to steric and strain factors. These features strongly influence the stability of the adduct with respect to the metal−ligand interaction.[4a,b] Of the numerous ligand types investigated, bipyridines and pyrazolylpyridines appear to be optimal since they are resistant to oxidative degradation or exchange reactions under the catalytic conditions. The adduct stabilities are mainly due to the strongly exothermic binding of the bidentate nitrogen-donor ligands.[4a]

In assessing the potential of $[MoO_2Cl_2(L)_n]$ complexes to be used in catalytic olefin epoxidation, the stability of the complexes under the reaction conditions is of critical importance. In previous work with a dichloro complex bearing 4,4′-di-*n*-hexyl-2,2′-bipyridine,[4c] it was found that the complex could be recovered unaltered after a catalytic run at 55 °C with *cis*-cyclooctene as the substrate. This indicated that the Mo−Cl bonds were not cleaved and that the catalytically active species existed in equilibrium with the starting complex in solution. By contrast, when complexes of the type $[MoO_2Cl_2(L)_2]$ bearing *N*,*N*-dialkylamides were examined as catalysts for the same reaction, dioxo(μ-oxo)molybdenum(VI) dimers of the type $[Mo_2O_4(\mu_2\text{-}O)Cl_2(L)_4]$ were formed, probably because of the presence of adventitious water (the supplied decane solution of TBHP may contain up to 4% water).[4d] Similarly, treatment of MoO_2Cl_2 with 2 equiv of pyrazole (pzH) monohydrate in THF at room temperature gave quantitative $[Mo_2O_4(\mu_2\text{-}O)Cl_2(pzH)_4]$ instead of mononuclear $[MoO_2Cl_2(pzH)_2]$.[7] The oxo-bridged dimer exhibited very high activity in the catalytic epoxidation of cyclic olefins. For the reaction of $[MoO_2Cl_2(H_2O)_2]\cdot Et_4NCl$ with 1 equiv of 4,4′-di-*tert*-butyl-2,2′-bipyridine (tbbpy),[8] the monomeric complex $[MoO_2Cl_2(tbbpy)]$ was obtained when the reaction was run in CH_2Cl_2, whereas the oxo-bridged dimer $[Mo_2O_4(\mu_2\text{-}O)Cl_2(tbbpy)_2]$ was the only reaction product when performed in a CH_2Cl_2/H_2O biphasic system. In recent work, the oxodiperoxo complex $[MoO(O_2)_2(tbbpy)]$ was isolated from the reaction of $[MoO_2Cl_2(tbbpy)]$ in water under microwave-assisted heating at 120 °C for 4 h.[9] These last four studies serve to illustrate that the Mo−Cl bond in $[MoO_2Cl_2(L)_n]$ complexes may be susceptible to cleavage under the reaction conditions typically employed for olefin epoxidation, and this should be investigated by isolating the Mo-containing species after catalytic runs and/or after treatment of the complexes with excess TBHP.

In the present work we describe the synthesis, characterization, and catalytic performance in olefin epoxidation of a dichlorodioxomolybdenum(VI) complex bearing 2-[3(5)-pyrazolyl]pyridine (PzPy). The recrystallization of $[MoO_2Cl_2(PzPy)]$ (**1**) under different conditions originated different crystal structures: one containing mononuclear **1** co-crystallized with a PzPyHCl salt, three containing oxo-bridged dimers of the type mentioned above, and one containing an anionic oxodiperoxomolybdenum(VI) complex with a weakly coordinated $PzPyH^+$ cation. These results led us to examine in more detail the Mo-containing species formed during catalytic runs using **1** as the starting complex, and for comparison the complex $[MoO_2(OSiPh_3)_2(PzPy)]$ was also prepared and tested in catalytic olefin epoxidation.

Experimental Section

Materials and Methods. Microanalyses for C, H, and N were performed at the Instituto de Tecnologia Química e Biológica (Lisbon, Portugal) using a Truspec, Leco equipment, and at the University of Aveiro. Quantification of molybdenum in the samples was performed at the Instituto Superior Técnico (Lisbon, Portugal) by inductively coupled plasma optical emission spectroscopy (ICP-OES) after acid digestion of the sample (10% experimental error). The FT-IR spectra were recorded on a Mattson 7000 FTIR spectrometer at room temperature, using a globar source, a DTGS detector, and potassium bromide cells, with 2 cm^{-1} resolution and triangular apodization. Attenuated total reflectance (ATR) FT-IR spectra were measured on the same instrument equipped with a Specac Golden Gate Mk II ATR accessory having a diamond top-plate and KRS-5 focusing lenses. The FT-Raman spectra were recorded at room temperature in the 70−4000 cm^{-1} range on an RFS-100 Bruker FT-spectrometer with 2 cm^{-1} resolution, using a Nd:YAG laser (Coherent Compass-1064/500) with an excitation wavelength of 1064 nm. A Bruker CXP 300 spectrometer was used to collect ^1H NMR spectra at room temperature. Chemical shifts are quoted in parts per million from tetramethylsilane.

SEM (Scanning Electron Microscopy) images and EDS (energy-dispersive X-ray spectroscopy) data were collected using a Hitachi SU-70 scanning electron microscope operating at 4 kV (for SEM and mapping) or 15 kV (for EDS). Samples were prepared by deposition on aluminum sample holders followed by carbon coating performed on an Emitech K 950 carbon evaporator. Powder X-ray diffraction (XRD) data were collected on a Philips X'pert MPD diffractometer equipped with an X'Celerator detector, a graphite monochromator ($Cu-K_\alpha$ X-radiation filtered by Ni (λ = 1.5418 Å)) and a flat-plate sample holder, in a Bragg−Brentano para-focusing optics configuration (40 kV, 50 mA). Samples were step-scanned in 0.02° 2θ steps with a counting time of 19.7 s per step.

(4) (a) Al-Ajlouni, A. M.; Günyar, A.; Zhou, M.-D.; Baxter, P. N. W.; Kühn, F. E. *Eur. J. Inorg. Chem.* **2009**, 1019–1026. (b) Günyar, A.; Zhou, M.-D.; Drees, M.; Baxter, P. N. W.; Bassioni, G.; Herdtweck, E.; Kühn, F. E. *Dalton Trans.* **2009**, 8746–8754. (c) Kühn, F. E.; Groarke, M.; Bencze, É.; Herdtweck, E.; Prazeres, A.; Santos, A. M.; Calhorda, M. J.; Romão, C. C.; Gonçalves, I. S.; Lopes, A. D.; Pillinger, M. *Chem.—Eur. J.* **2002**, *8*, 2370–2383. (d) Gago, S.; Neves, P.; Monteiro, B.; Pessêgo, M.; Lopes, A. D.; Valente, A. A.; Paz, F. A. A.; Pillinger, M.; Moreira, J.; Silva, C. M.; Gonçalves, I. S. *Eur. J. Inorg. Chem.* **2009**, 4528–4537. (e) Bruno, S. M.; Pereira, C. C. L.; Balula, M. S.; Nolasco, M.; Valente, A. A.; Hazell, A.; Pillinger, M.; Ribeiro-Claro, P.; Gonçalves, I. S. *J. Mol. Catal. A: Chem.* **2007**, *261*, 79–87. (f) Bruno, S. M.; Fernandes, J. A.; Martins, L. S.; Gonçalves, I. S.; Pillinger, M.; Ribeiro-Claro, P.; Rocha, J.; Valente, A. A. *Catal. Today* **2006**, *114*, 263–271. (g) Santos, A. M.; Kühn, F. E.; Bruus-Jensen, K.; Lucas, I.; Romão, C. C.; Herdtweck, E. *J. Chem. Soc., Dalton Trans.* **2001**, *8*, 1332–1337. (h) Petrovski, Ž.; Pillinger, M.; Valente, A. A.; Gonçalves, I. S.; Hazell, A.; Romão, C. C. *J. Mol. Catal. A: Chem.* **2005**, *227*, 67–73. (i) Jimtaisong, A.; Luck, R. L. *Inorg. Chem.* **2006**, *45*, 10391–10402. (j) Kühn, F. E.; Lopes, A. D.; Santos, A. M.; Herdtweck, E.; Haider, J. J.; Romão, C. C.; Santos, A. G. *J. Mol. Catal. A: Chem.* **2000**, *151*, 147–160. (k) Valente, A. A.; Moreira, J.; Lopes, A. D.; Pillinger, M.; Nunes, C. D.; Romão, C. C.; Kühn, F. E.; Gonçalves, I. S. *New J. Chem.* **2004**, *28*, 308–313. (l) Gago, S.; Rodríguez-Borges, J. E.; Teixeira, C.; Santos, A. M.; Zhao, J.; Pillinger, M.; Nunes, C. D.; Petrovski, Z.; Santos, T. M.; Kühn, F. E.; Romão, C. C.; Gonçalves, I. S. *J. Mol. Catal. A: Chem.* **2005**, *236*, 1–6. (m) Al-Ajlouni, A.; Valente, A. A.; Nunes, C. D.; Pillinger, M.; Santos, A. M.; Zhao, J.; Romão, C. C.; Gonçalves, I. S.; Kühn, F. E. *Eur. J. Inorg. Chem.* **2005**, 1716–1723. (n) Bruno, S. M.; Monteiro, B.; Balula, M. S.; Pedro, F. M.; Abrantes, M.; Valente, A. A.; Pillinger, M.; Ribeiro-Claro, P.; Kühn, F. E.; Gonçalves, I. S. *J. Mol. Catal. A: Chem.* **2006**, *260*, 11–18. (o) Bruno, S. M.; Balula, S. S.; Valente, A. A.; Paz, F. A. A.; Pillinger, M.; Sousa, C.; Klinowski, J.; Freire, C.; Ribeiro-Claro, P.; Gonçalves, I. S. *J. Mol. Catal. A: Chem.* **2007**, *270*, 185–194. (p) Günyar, A.; Kühn, F. E. *J. Mol. Catal. A: Chem.* **2010**, *319*, 108–113.

(5) Barea, G.; Lledos, A.; Maseras, F.; Jean, Y. *Inorg. Chem.* **1998**, *37*, 3321–3325.

(6) For a recent review see: Sanz, R.; Pedrosa, M. R. *Curr. Org. Synth.* **2009**, *6*, 239–263.

(7) Pereira, C. C. L.; Balula, S. S.; Paz, F. A. A.; Valente, A. A.; Pillinger, M.; Klinowski, J.; Gonçalves, I. S. *Inorg. Chem.* **2007**, *46*, 8508–8510.

(8) Arzoumanian, H.; Bakhtchadjian, R.; Agrifoglio, G.; Atencio, R.; Briceño, A. *Transition Met. Chem.* **2006**, *31*, 681–689.

(9) Amarante, T. R.; Paz, F. A. A.; Gago, S.; Gonçalves, I. S.; Pillinger, M.; Rodrigues, A. E.; Abrantes, M. *Molecules* **2009**, *14*, 3610–3620.

Scheme 1. Preparation of $MoO_2(OSiPh_3)_2$, $[MoO_2Cl_2(THF)_2]$, and Complexes **1** and **5**, and Atom Numbering for the NMR Assignments

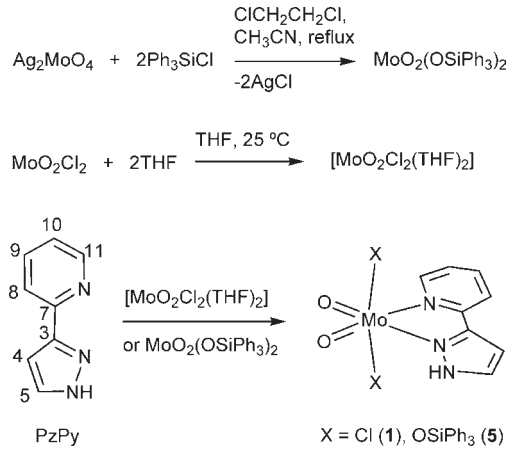

Air-sensitive procedures were performed using standard Schlenk techniques under nitrogen atmosphere. Microwave-assisted heating was carried out in a Discover S-Class (CEM Corporation, U.S.A.) microwave oven, at 2.45 GHz, under stirring and simultaneous cooling with compressed air (20 psi) to prevent bulk overheating. A vertical focused IR sensor was used for temperature measurement. MoO_2Cl_2, anhydrous THF and 1,2-dichloroethane, *n*-hexane, dichloromethane, and diethyl ether were purchased from Sigma-Aldrich and used as received. 2-[3(5)-Pyrazolyl]pyridine (PzPy)[10] and $[MoO_2(OSiPh_3)_2]$[4e] were prepared using published procedures. ^{1}H NMR data for PzPy (DMSO-d_6, 300 MHz,): δ (ppm) = 13.1 (vbr s, N−H), 8.58 (d, 1H, 11-H), 7.93 (d, 1H, 8-H), 7.84 (t, 1H, 9-H), 7.76 (br s, 1H, 5-H), 7.30 (dd, 1H, 10-H), 6.85 (s, 1H, 4-H) (see Scheme 1 for atom numbering).

[MoO_2Cl_2(PzPy)] (1). MoO_2Cl_2 (0.34 g, 1.72 mmol) was dissolved in dry THF (10 mL) to prepare a solution of the solvent adduct $[MoO_2Cl_2(THF)_2]$. The ligand PzPy (0.25 g, 1.72 mmol) was added with stirring, which resulted in the formation of a precipitate. The suspension was stirred at 50 °C for 3 h. After filtering off the solution, dichloromethane (10 mL) was added to the solid, and the mixture stirred for 20 min at room temperature. *n*-Pentane (10 mL) was then added to complete the precipitation of the crude product, which was filtered, washed with *n*-pentane, and vacuum-dried to give **1** as a yellow solid (0.55 g, 93%). Anal. Calcd for $C_8H_7Cl_2MoN_3O_2$: C, 27.93; H, 2.05; N, 12.21. Found: C, 28.36; H, 2.03; N, 11.92. Selected IR (KBr, cm^{-1}): 345 m, 395w, 430vw, 483vw, 507vw, 595w, 645w, 708w, 785 m, 805sh, 906vs, 928w, 940s, 977w, 1024w, 1069vw, 1094w, 1110sh, 1146w, 1204vw, 1254vw, 1297w, 1375 m, 1431 m, 1465w, 1512w, 1534w, 1567vw, 1612s, 3044vw, 3113 m, 3125 m, 3258 m. Selected Raman (cm^{-1}): 171w, 222 m, 247 m, 310 m, 370w, 397 m, 647w, 712w, 909s, 927 m, 937vs, 977w, 1024s, 1055w, 1070vw, 1097w, 1112vw, 1147w, 1156sh, 1200vw, 1253vw, 1315 m, 1376 m, 1432w, 1452 m, 1471w, 1517w, 1536vs, 1569s, 1612vs, 1625sh, 3065sh, 3075sh, 3085sh, 3115 m, 3127 m. ^{1}H NMR (DMSO-d_6, 300 MHz): δ (ppm) = 13.0 (br, N−H), 8.66 (d, 1H, 11-H), 8.19 (c, 2H, 8,9-H), 7.90 (d, 1H, 5-H), 7.58 (m, 1H, 10-H), 7.09 (d, 1H, 4-H).

Despite carrying out various attempts, single crystals of **1** suitable for X-ray diffraction could not be obtained, and instead the different recrystallization procedures led to low yields (5−20%) of either mononuclear $[MoO_2Cl_2(PzPy)]$ co-crystallized with a free (protonated) organic ligand (**2**), oxo-bridged dimers (**3a** and **3b**) or an oxodiperoxomolybdenum(VI) complex with a weakly coordinated (and protonated) 2-[3(5)-pyrazolyl]-pyridine (**4**). Details about the preparation of these crystals and selected characterization data are given below.

(10) Brunner, H.; Scheck, T. *Chem. Ber.* **1992**, *125*, 701–709.

[MoO_2Cl_2(PzPy)]·PzPyHCl (2). MoO_2Cl_2 (0.14 g, 0.69 mmol) was dissolved in dry THF (15 mL) to prepare a solution of the solvent adduct $[MoO_2Cl_2(THF)_2]$. After evaporating the solution to dryness, dichloromethane (30 mL) and PzPy (0.10 g, 0.69 mmol) were added, and the suspension was stirred at room temperature for 20 min. The resultant yellow solution was filtered off, layered with diethyl ether, and allowed to stand for 2 weeks, whereupon a small crop of yellow crystals of **2** were obtained (20 mg, 6% (based on Mo)). Anal. Calcd for $C_{16}H_{15}Cl_3MoN_6O_2$: C, 36.56; H, 2.88; N, 15.99. Found: C, 36.57; H, 3.27; N, 15.96. Selected IR (KBr, cm^{-1}): 332s, 393w, 423vw, 448 m, 615 m, 741 m, 768vs, 916s, 939s, 1066w, 1091 m, 1159 m, 1183 m, 1205 m, 1243vs, 1291 m, 1312 m, 1363 m, 1380w, 1435 m, 1455w, 1487w, 1512 m, 1543w, 1569vw, 1612vs, 1626s, 3104 m, 3260s, 3309 m, 3391br.

[$Mo_2O_4(\mu_2$-O)Cl_2(PzPy)$_2$] (3a−c). A small crop (7 mg, 8%) of brown crystals of **3a** were obtained by slow diffusion of diethyl ether vapor into a solution of **1** (0.10 g, 0.29 mmol) in acetonitrile (20 mL) over a period of about 1 month. Anal. Calcd for $C_{16}H_{14}Cl_2Mo_2N_6O_5$: C, 30.35; H, 2.23; N, 13.27. Found: C, 30.77; H, 2.25; N, 13.44. Selected IR (KBr, cm^{-1}): 335 m, 345sh, 371w, 394w, 431w, 448w, 483vw, 506vw, 594vw, 616w, 643w, 710w, 773sh, 785s, 808sh, 906vs, 928w, 942s, 977w, 1024 m, 1054w, 1070 m, 1094 m, 1108sh, 1148 m, 1162vw, 1184w, 1208w, 1254w, 1297 m, 1315w, 1364 m, 1376sh, 1432 m, 1466w, 1516 m, 1534 m, 1560vw, 1570w, 1612s, 1626 m, 3036vw, 3109 m, 3125 m, 3252 m. Selected Raman (cm^{-1}): 166vw, 222 m, 231sh, 245sh, 285w, 306 m, 364w, 395 m, 647w, 700w, 712w, 890sh, 907w, 929 m, 936 m, 945sh, 976w, 1022 m, 1055w, 1070vw, 1097vw, 1147w, 1165sh, 1198vw, 1253sh, 1318 m, 1365sh, 1376 m, 1434sh, 1453 m, 1467 m, 1517w, 1536vs, 1569s, 1611vs, 1625sh, 3070sh, 3085sh, 3093sh, 3111 m, 3126 m. The use of dichloromethane instead of acetonitrile in the above procedure gave a small crop of yellow crystals of **3b**.

In an attempt to obtain a higher yield of the oxo-bridged dimer, complex **1** (0.15 g, 0.44 mmol) was suspended in a mixture of THF (5 mL), diglyme (5 mL), and 0.5 equiv of H_2O (4 μL). Microwave-assisted heating of the suspension at 120 °C for 30 min gave a clear yellow solution. After cooling the solution to room temperature, it was layered with diethyl ether and left to stand for 4 months, at which point a small crop of yellow crystals of **3c** were collected.

[$MoO(O_2)_2$Cl(PzPyH)] (4). Crystals of this compound were repeatedly obtained after carrying out recrystallizations over long periods. For example, colorless crystals of **4** (20 mg, 19%) were obtained after slow diffusion of diethyl ether vapor into a solution of **1** (0.10 g, 0.29 mmol) in either acetonitrile or dichloromethane (20 mL) over a period of about 5 months. Anal. Calcd for $C_8H_8ClMoN_3O_5$: C, 26.87; H, 2.25; N, 11.75. Found: C, 26.92; H, 2.15; N, 11.43. Selected IR (KBr, cm^{-1}): 349 m, 454 m, 504w, 540 m, 580s, 624 m, 648 m, 682vw, 700vw, 731vw, 770s, 794w, 858s, 874sh, 955 m, 985s, 1058 m, 1087 m, 1102 m, 1164 m, 1200 m, 1254sh, 1307 m, 1351 m, 1377w, 1443 m, 1492 m, 1505 m, 1548w, 1617s, 1632s, 2855w, 2925w, 3100w, 3131 m, 3287 m. Selected Raman (cm^{-1}): 184 m, 239sh, 267sh, 293w, 312w, 327 m, 348w, 365 m, 392sh, 457w, 504w, 543s, 584 m, 627 m, 648w, 703 m, 714w, 877s, 929 m, 953 m, 992s, 1013sh, 1049w, 1090vw, 1136w, 1163w, 1233sh, 1258sh, 1292 m, 1316sh, 1352 m, 1366sh, 1437vs, 1495s, 1527 m, 1547sh, 1570s, 1610s, 1634vs, 3077sh, 3098 m, 3117sh, 3135 m cm^{-1}. ^{1}H NMR (DMSO-d_6, 300 MHz): δ (ppm) = 8.68 (d, 1H, 11-H), 8.34 (br, 1H, N−H), 7.95 (d, 1H, 8-H), 7.87 (t, 1H, 9-H), 7.76 (br s, 1H, 5-H), 7.42 (dd, 1H, 10-H), 6.87 (d, 1H, 4-H).

[MoO_2(OSiPh$_3$)$_2$(PzPy)] (5). A suspension of Ag_2MoO_4 (0.70 g, 1.86 mmol) in 1,2-dichloroethane (35 mL) and CH_3CN (3 mL) was stirred for 15 min at room temperature. Ph_3SiCl (1.10 g, 3.73 mmol) was then added, and the mixture was refluxed under nitrogen for 8 h. The solution was filtered off at room temperature and treated with PzPy (0.27 g, 1.86 mmol). After stirring for 3 h at room temperature, the solution was

filtered and evaporated to dryness. The resultant white solid was washed with diethyl ether (2 × 15 mL), hexane (2 × 10 mL), and vacuum-dried (0.99 g, 75%). Anal. Calcd for $C_{44}H_{37}MoN_3O_4Si_2$: C, 64.14; H, 4.53; N, 5.10. Found: C, 64.91; H, 4.31; N, 5.10. Selected IR (KBr, cm^{-1}): 278 m, 293vw, 304vw, 329 m, 342sh, 372w, 382w, 430w, 462w, 513s, 535w, 560w, 582w, 621w, 641w, 653w, 678sh, 698sh, 710s, 741 m, 770 m, 777sh, 796vw, 841 m, 904sh, 925vs, 970w, 997w, 1007w, 1020vw, 1030w, 1050sh, 1062w, 1090w, 1113s, 1142w, 1155 m, 1187 m, 1203w, 1223sh, 1231vw, 1251sh, 1261w, 1296sh, 1305w, 1334vw, 1376 m, 1429 m, 1452sh, 1459w, 1484w, 1509w, 1529w, 1568w, 1588 m, 1607 m, 2977sh, 2999w, 3011sh, 3021sh, 3050 m, 3065 m, 3131w, 3143w, 3349 m. Selected Raman (cm^{-1}): 196w, 238w, 283sh, 293w, 330w, 383 m, 430vw, 535vw, 618w, 639vw, 678w, 711w, 745sh, 796sh, 881sh, 904 m, 925 m, 968w, 998vs, 1029 m, 1051vw, 1106 m, 1158 m, 1187 m, 1252vw, 1312 m, 1377w, 1429sh, 1447w, 1460 m, 1479sh, 1508w, 1529s, 1568s, 1590vs, 1605 m, 1609sh, 2998sh, 3046sh, 3052vs, 3133w, 3142sh, 3174w. ^{1}H NMR (acetone-d_6, 300 MHz): δ (ppm) = 12.5 (br, N−H), 8.60 (d, 1H, 11-H), 7.83 (t, 1H, 9-H), 7.66−7.64 (c, 12H, phenyl-H), 7.48 (d, 1H, 8-H), 7.46−7.38 (c, 18H, phenyl-H), 7.31−7.27 (m, 1H, 5-H), 6.93 (d, 1H, 10-H), 6.05 (d, 1H, 4-H). Suitable crystals for X-ray diffraction were obtained by slow evaporation of a saturated solution of **5** in CH_2Cl_2.

DFT Calculations. DFT calculations were performed using the G03W program package[11] running on a personal computer. The fully optimized geometry, the harmonic vibrational wavenumbers, and the infrared and Raman intensities were obtained at the B3LYP level, using the standard LanL2DZ basis set and effective core potentials. To obtain the best fit with experimental values, the harmonic vibrational wavenumbers were scaled by a factor of 0.961.[12] Because of the large size of the systems, the phenyl groups were replaced by H atoms in complex **5**. Previous calculations have shown that the calculated wavenumbers around the Mo center are not significantly affected by this approach.[4e,13] The vibrational assignments were based on the atomic displacements and calculated intensities.

Single-Crystal X-ray Diffraction. Suitable single-crystals of $[MoO_2Cl_2(PzPy)]\cdot PzPyHCl$ (**2**), $[Mo_2O_4(\mu_2\text{-}O)Cl_2(PzPy)_2]\cdot CH_3CN$ (**3a**), $[Mo_2O_4(\mu_2\text{-}O)Cl_2(PzPy)_2]$ (**3b**), $[Mo_2O_4(\mu_2\text{-}O)Cl_2(PzPy)_2]\cdot 2THF$ (**3c**), $[MoO(O_2)_2Cl(PzPyH)]$ (**4**), and $[MoO_2(OSiPh_3)_2(PzPy)]$ (**5**) were manually harvested from the crystallization vials and mounted on either glass fibers or CryoLoops (Hampton Research) using highly viscous FOMBLIN Y perfluoropolyether vacuum oil (LVAC 140/13, Aldrich) to avoid degradation because of the evaporation of the solvent molecules.[14]

Single-crystal data for compounds **3a** and **5** were collected on a Nonius Kappa CCD area-detector diffractometer (Mo K_α graphite-monochromated radiation, $\lambda = 0.71073$ Å), equipped with an Oxford Cryosystems cryostream and controlled by the Collect software package.[15] Images were processed using the software packages Denzo and Scalepack,[16] and data were corrected for absorption by the empirical method employed in Sortav.[17] Data for the remaining compounds were collected on a Bruker X8 Kappa APEX II CCD area-detector diffractometer (Mo K_α graphite-monochromated radiation, $\lambda = 0.71073$ Å) controlled by the APEX2 software package,[18] and equipped with an Oxford Cryosystems Series 700 cryostream monitored remotely using Cryopad.[19] Images were processed using SAINT+,[20] and data were corrected for absorption by the multiscan semi-empirical method implemented in SADABS.[21] All structures were solved by the direct methods of SHELXS-97,[22] and refined by full-matrix least-squares on F^2 using SHELXL-97.[22a,23] All non-hydrogen atoms were directly located from difference Fourier maps and refined, when possible, using anisotropic displacement parameters.

Hydrogen atoms bound to carbon were located at their idealized positions using the HFIX 43 instruction in SHELXL and included in subsequent refinement cycles in riding-motion approximation with an isotropic thermal displacement parameter (U_{iso}) fixed at 1.2 × U_{eq} of the attached carbon atom. While a similar procedure was adopted for the location of the hydrogen atom bound to nitrogen associated with the PzPy moieties in **3b**, **3c**, and **4**, in compounds **2**, **3a**, and **5** the same hydrogen was instead directly located from difference Fourier maps and included in the final structural model with the N−H distance restrained to 0.95(1) or 1.00(1) Å and with $U_{iso} = 1.5 \times U_{eq}$(N).

In compound **3a** one coordinated 2-[3(5)-pyrazolyl]pyridine molecule was found to be disordered over two distinct crystallographic positions which are mutually rotated by about 180°: the pyridine and pyrazole rings of each fraction were found to be almost overlapped. This disorder was modeled into the final structure with heavily constrained molecular geometries to ensure chemically reasonable environments for these moieties: (i) equivalent bonds for the two fractions were constrained to be identical; (ii) Mo−N distances to pyridine and pyrazole rings were constrained to similar, but refineable, values; (iii) non-hydrogen atoms for the two fractions were refined by assuming an identical isotropic thermal displacement parameter. After full structural refinement the two fractions of the disordered PzPy molecule converged to 45.9(6) and 54.1(4)%.

Some phenyl groups associated with the crystallographically independent complex $[MoO_2(OSiPh_3)_2(PzPy)]$ in **5** were found to be affected by thermal disorder. On the one hand, all carbon atoms composing the C(15)→C(20) aromatic ring were constrained to lie on the same average plane by employing the FLAT instruction in SHELXL. On the other, the C(21)→C(26) aromatic ring was found to be disordered over two distinct

(11) Frisch, M. J.; Trucks, G. W.; Schlegel, H. B.; Scuseria, G. E.; Robb, M. A.; Cheeseman, J. R.; Montgomery, Jr., J. A.; Vreven, T.; Kudin, K. N.; Burant, J. C.; Millam, J. M.; Iyengar, S. S.; Tomasi, J.; Barone, V.; Mennucci, B.; Cossi, M.; Scalmani, G.; Rega, N.; Petersson, G. A.; Nakatsuji, H.; Hada, M.; Ehara, M.; Toyota, K.; Fukuda, R.; Hasegawa, J.; Ishida, M.; Nakajima, T.; Honda, Y.; Kitao, O.; Nakai, H.; Klene, M.; Li, X.; Knox, J. E.; Hratchian, H. P.; Cross, J. B.; Bakken, V.; Adamo, C.; Jaramillo, J.; Gomperts, R.; Stratmann, R. E.; Yazyev, O.; Austin, A. J.; Cammi, R.; Pomelli, C.; Ochterski, J. W.; Ayala, P. Y.; Morokuma, K.; Voth, G. A.; Salvador, P.; Dannenberg, J. J.; Zakrzewski, V. G.; Dapprich, S.; Daniels, A. D.; Strain, M. C.; Farkas, O.; Malick, D. K.; Rabuck, A. D.; Raghavachari, K.; Foresman, J. B.; Ortiz, J. V.; Cui, Q.; Baboul, A. G.; Clifford, S.; Cioslowski, J.; Stefanov, B. B.; Liu, G.; Liashenko, A.; Piskorz, P.; Komaromi, I.; Martin, R. L.; Fox, D. J.; Keith, T.; Al-Laham, M. A.; Peng, C. Y.; Nanayakkara, A.; Challacombe, M.; Gill, P. M. W.; Johnson, B.; Chen, W.; Wong, M. W.; Gonzalez, C.; Pople, J. A. *Gaussian 03*, Revision B.04; Gaussian, Inc.: Wallingford, CT, 2003.

(12) Johnson III, R. D., Ed.; NIST Computational Chemistry Comparison and Benchmark Database, NIST Standard Reference Database Number 101, Release 12, Aug 2005; http://srdata.nist.gov/cccbdb.

(13) Bruno, S. M.; Monteiro, B.; Balula, M. S.; Lourenço, C.; Valente, A. A.; Pillinger, M.; Ribeiro-Claro, P.; Gonçalves, I. S. *Molecules* **2006**, *11*, 298–308.

(14) Kottke, T.; Stalke, D. *J. Appl. Crystallogr.* **1993**, *26*, 615–619.

(15) Hooft, R. *Collect: Data Collection Software*; Nonius B. V.: Delft, The Netherlands, 1998.

(16) Otwinowski, Z.; Minor, W. *Methods Enzymol.*; Carter Jr., C. W., Sweet, R. M., Eds.; Academic Press: New York, 1997; Vol. *276*, p 307.

(17) (a) Blessing, R. H. *Acta Crystallogr., Sect. A: Found. Crystallogr.* **1995**, *51*, 33–38. (b) Blessing, R. H. *J. Appl. Crystallogr.* **1997**, *30*, 421–426.

(18) *APEX2 Data Collection Software*, version 2.1-RC13; Bruker AXS: Delft, The Netherlands, 2006.

(19) *Cryopad, Remote monitoring and control*, version 1.451; Oxford Cryosystems: Oxford, United Kingdom, 2006.

(20) *SAINT+ Data Integration Engine*, version 7.23a; Bruker AXS: Madison, WI, 2005.

(21) Sheldrick, G. M. *SADABS*, version 2.01; Bruker AXS: Madison, WI, 1998.

(22) (a) Sheldrick, G. M. *Acta Crystallogr., Sect. A: Found. Crystallogr.* **2008**, *64*, 112–122. (b) Sheldrick, G. M. *SHELXS-97, Program for Crystal Structure Solution*; University of Göttingen: Göttingen, Germany, 1997.

(23) Sheldrick, G. M. *SHELXL-97, Program for Crystal Structure Refinement*; University of Göttingen: Göttingen, Germany, 1997.

Table 1. Crystal and Structure Refinement Data for Compounds **2** to **5**

	2	**3a**	**3b**	**3c**	**4**	**5**
formula	$C_{16}H_{15}Cl_3MoN_6O_2$	$C_{18}H_{17}Cl_2Mo_2N_7O_5$	$C_{16}H_{14}Cl_2Mo_2N_6O_5$	$C_{24}H_{30}Cl_2Mo_2N_6O_7$	$C_8H_8ClMoN_3O_5$	$C_{44}H_{37}MoN_3O_4Si_2$
formula weight	525.63	674.17	633.11	777.32	357.56	823.89
temperature/K	150(2)	120(2)	180(2)	150(2)	100(2)	120(2)
crystal system	monoclinic	monoclinic	triclinic	monoclinic	monoclinic	monoclinic
space group	$C2/c$	$P2_1/c$	$P\bar{1}$	$P2_1/n$	$P2_1/c$	$P2_1/n$
a/Å	25.1428(8)	10.856(2)	7.5738(7)	8.4171(3)	8.9171(15)	9.3906(19)
b/Å	8.2630(3)	12.715(3)	7.8222(6)	14.0198(5)	6.6239(10)	26.954(5)
c/Å	19.8535(7)	16.935(3)	10.1283(8)	13.1235(4)	19.872(3)	15.527(3)
α/deg			69.032(4)			
β/deg	95.3200(10)	93.74(3)	83.840(4)	100.594(2)	97.371(7)	96.07(3)
γ/deg			73.941(4)			
volume/Å^3	4106.9(2)	2332.6(8)	538.42(8)	1522.25(9)	1164.1(3)	3908.0(14)
Z	8	4	1	2	4	4
D_c/g cm^{-3}	1.700	1.920	1.953	1.696	2.040	1.400
μ(Mo−Kα)/mm^{-1}	1.054	1.350	1.454	1.051	1.373	0.444
F(000)	2096	1328	310	780	704	1696
crystal size/mm	0.20 × 0.16 × 0.14	0.21 × 0.12 × 0.07	0.08 × 0.06 × 0.06	0.20 × 0.08 × 0.06	0.10 × 0.10 × 0.04	0.14 × 0.05 × 0.02
crystal type	yellow prisms	brown blocks	yellow blocks	yellow needles	colorless plates	white blocks
θ range	3.55 to 36.35	3.54 to 27.51	3.52 to 25.35	3.81 to 29.13	3.71 to 29.13	3.58 to 27.50
index ranges	$-41 \le h \le 41$ $-13 \le k \le 13$ $-33 \le l \le 28$	$-14 \le h \le 14$ $-16 \le k \le 16$ $-18 \le l \le 21$	$-9 \le h \le 9$ $-9 \le k \le 9$ $-12 \le l \le 12$	$-11 \le h \le 11$ $-19 \le k \le 19$ $-16 \le l \le 17$	$-12 \le h \le 12$ $-8 \le k \le 8$ $-27 \le l \le 27$	$-12 \le h \le 12$ $-34 \le k \le 34$ $-18 \le l \le 20$
reflections collected	42926	12968	14234	71630	39382	18189
independent reflections	9914 (R_{int} = 0.0386)	5328 (R_{int} = 0.0340)	1965 (R_{int} = 0.0276)	4084 (R_{int} = 0.0520)	3115 (R_{int} = 0.0346)	8528 (R_{int} = 0.0529)
final R indices $[I > 2\sigma(I)]$[a,b]	$R1$ = 0.0313 $wR2$ = 0.0725	$R1$ = 0.0590 $wR2$ = 0.1289	$R1$ = 0.0252 $wR2$ = 0.0551	$R1$ = 0.0332 $wR2$ = 0.055	$R1$ = 0.0575 $wR2$ = 0.1466	$R1$ = 0.0663 $wR2$ = 0.1331
final R indices (all data)[a,b]	$R1$ = 0.0420 $wR2$ = 0.0762	$R1$ = 0.0684 $wR2$ = 0.1331	$R1$ = 0.0274 $wR2$ = 0.0562	$R1$ = 0.0534 $wR2$ = 0.0720	$R1$ = 0.0627 $wR2$ = 0.1487	$R1$ = 0.0970 $wR2$ = 0.1475
weighting scheme[c]	m = 0.0203 n = 5.2216	m = 0 n = 17.9162	m = 0.0125 n = 1.1613	m = 0.0271 n = 1.4986	m = 0.0356 n = 15.7473	m = 0.0299 n = 14.7265
largest diff. peak and hole	1.095 and −1.175 e Å^{-3}	1.360 and −1.020 e Å^{-3}	0.917 and −0.725 e Å^{-3}	0.561 and −0.799 e Å^{-3}	4.181 and −1.090 e Å^{-3}	1.075 and −0.645 e Å^{-3}
CCDC deposition No.	765533	765534	657133	765535	765536	657134

[a] $R1 = \sum||F_o| - |F_c||/\sum|F_o|$. [b] $wR2 = [\sum w(F_o^2 - F_c^2)^2/\sum w(F_o^2)^2]^{1/2}$. [c] $w = 1/[\sigma^2(F_o^2) + (mP)^2 + nP]$ where $P = (F_o^2 + 2F_c^2)/3$.

crystallographic positions [C(21A)→C(26A) and C(21B)→C(26B)], which were included in the final structural model with a heavily restrained geometry (i.e., independent FLAT instructions were used for each position of the aromatic ring), with the Si−C distances to C(21A) and C(21B) restrained to a common value, and with all carbon atoms being refined by assuming a common isotropic displacement parameter. The occupancy factor for each crystallographic position was included in the least-squares refinement cycles as a refineable variable which ultimately converged to 54.8(6)% and 45.2(6)%.

The last difference Fourier map synthesis showed the following: for **2**, the highest peak (1.095 e Å^{-3}) and deepest hole (−1.175 e Å^{-3}) located at 0.56 Å and 0.50 Å from Mo(1), respectively; for **3a**, the highest peak (1.360 e Å^{-3}) and deepest hole (−1.020 e Å^{-3}) located at 1.12 Å and 0.84 Å from C(15) and Mo(1), respectively; for **3b**, the highest peak (0.917 e Å^{-3}) and deepest hole (−0.725 e Å^{-3}) located at 0.81 Å and 0.71 Å from Mo(1), respectively; for **3c**, the highest peak (0.561 e Å^{-3}) and deepest hole (−0.799 e Å^{-3}) located at 0.71 Å and 0.73 Å from Mo(1), respectively; for **4**, the highest peak (4.181 e Å^{-3}) and deepest hole (−1.090 e Å^{-3}) located at 1.16 Å and 1.32 Å from Mo(1) and C(4), respectively; for **5**, the highest peak (1.075 e Å^{-3}) and deepest hole (−0.645 e Å^{-3}) located at 1.12 Å from C(7) and 0.78 Å from Mo(1), respectively.

Table 1 lists the crystallographic data collection and structure refinement details, and Cambridge Crystallographic Data Centre (CCDC) deposition numbers. Bond lengths and angles for the Mo^{VI} coordination environments and {SiC_3O} tetrahedra, and geometric details of the hydrogen bonding in all structures, are provided as Supporting Information. Copies of the crystallographic data (excluding structure factors) can be obtained free of charge on application to CCDC, 12 Union Road, Cambridge CB2 1EZ, U.K. (fax: +44 (0) 1223 336033; e-mail: deposit@ccdc.cam.ac.uk).

Catalysis. The liquid-phase catalytic epoxidation reactions were carried out under air (atmospheric pressure) with magnetic stirring (800 rpm) in closed borosilicate reaction vessels (5 mL capacity) immersed in a thermostatted oil bath (55 °C). Typically, the reaction vessel was loaded with the metal complex corresponding to 0.018 mmol of molybdenum, 1.8 mmol of *cis*-cyclooctene (Cy), 2.75 mmol of oxidant (5.5 M TBHP in decane, which contains up to 4 wt % H_2O), and no additional co-solvent. To recover the solid phase, the reaction mixture was cooled to room temperature, and the solid was separated by centrifugation (3500 rpm), washed with *n*-hexane, and dried at room temperature overnight. The recovered solids were used in a second 24 h run, and the mass ratios of olefin/oxidant:catalyst were the same as those used in the first run. The leaching tests were carried out by performing the reaction of Cy with TBHP in decane, in the presence of solid catalyst, for 1 h at 55 °C, followed by filtering of the reaction mixture (at 55 °C) through a 0.2 μm PVDF w/GMF Whatman membrane. The filtrate was then stirred for a further 5 h at 55 °C (without adding any additional olefin or oxidant).

Reaction courses were monitored using a Varian 3900 GC equipped with a capillary column (DB-5, 30 m × 0.25 mm) and a flame ionization detector. Products were identified by GC-MS

(HP 5890 Series II GC; HP 5970 Series Mass Selective Detector) using He as the carrier gas.

Results and Discussion

Synthesis. The dichlorodioxomolybdenum(VI) complex **1** precipitated as a yellow solid upon addition of 2-[3(5)-pyrazolyl]pyridine (PzPy) to a solution of $[MoO_2Cl_2(THF)_2]$ in THF (Scheme 1). To get a better assessment of the influence of the anionic X ligand on catalytic performance, the corresponding triphenylsiloxy complex **5** was prepared by reacting silver molybdate with 2 equiv of Ph_3SiCl to give $MoO_2(OSiPh_3)_2$, followed by addition of PzPy. Complexes **1** and **5** were characterized by FTIR and FT-Raman spectroscopy, and ^1H NMR, and both exhibit data in line with those previously reported for analogous complexes.[4e,f] The full assignment of the vibrational spectra is described in more detail below. A comparison of the ^1H NMR spectra of PzPy and complex **1** (recorded in DMSO-d_6) shows that the resonances for the pyrazolylpyridine protons shift downfield by 0.08−0.35 ppm upon complexation, similar to that reported previously for the ligand ethyl[3-(2-pyridyl)-1-pyrazolyl]-acetate.[4f] Conversely, the same comparison for complex **5** reveals that the resonances are either unshifted (9,11-H) or shifted to higher field by 0.2−0.8 ppm (4,5,8,10-H). These differences suggest that the PzPy ligand is more weakly coordinated in complex **5** compared with **1**, which might be due to the steric crowding introduced by the bulky Ph_3SiO groups. These weak interactions have been observed in the crystallographic studies (see below). Additionally, the donor power of the triphenyl siloxy group is higher than that for Cl, which may lead to a more electron-rich metal center.[24]

Complex **1** is insoluble in nonpolar solvents such as diethyl ether and *n*-pentane, somewhat soluble in polar solvents such as dichloromethane, acetonitrile, and THF, and soluble in dimethylsulfoxide (DMSO). The low solubility meant that long recrystallization times were required using either vapor or solvent diffusion techniques (Et_2O/CH_2Cl_2, Et_2O/CH_3CN, or Et_2O/THF), and in no case were we able to isolate single crystals of **1** with a structure containing only six-coordinate $[MoO_2Cl_2(PzPy)]$ complexes. When a solution of **1** in CH_2Cl_2 was layered with Et_2O, a small crop of yellow crystals were obtained after two weeks. The crystallographic study (described below) revealed a structure comprising mononuclear $[MoO_2Cl_2(PzPy)]$ complexes co-crystallized with pyrazolylpyridinium chloride (PzPyHCl) (**2**). Recrystallization by vapor diffusion required even longer times (up to 5 months) and led to crystals that were identified by X-ray diffraction as being either oxo-bridged dimers of the type $[Mo_2O_4(\mu_2\text{-}O)Cl_2(PzPy)_2]$ (**3a** and **3b**) or the oxodiperoxo complex $[MoO(O_2)_2Cl(PzPyH)]$ (**4**). As will be described in more detail below, the structure of **4** is unique in having an $MoO(O_2)_2$ moiety coordinated to Cl; the organic ligand is protonated at the pyridyl-N atom and is only weakly associated with the $[MoO(O_2)_2Cl]^-$ anion. In contrast to compounds **2** and **3**, species **4** was reproducibly obtained after long (>4 months) recrystallization times, and this allowed enough material to be obtained for characterization by elemental analysis, vibrational spectroscopy, and ^1H NMR. It was not surprising to find that the ^1H NMR spectrum of **4** in DMSO-d_6 showed the presence of free ligand; the use of a noncoordinating solvent was not possible because of the very low solubility of **4**. For species **3** and **4** the presence of adventitious water and/or oxygen presumably led to the breaking of one Mo−Cl bond and, in the case of **4**, the eventual introduction of peroxo ligands. Attempts to obtain higher yields of **3** and **4** by treatment of **1** with either water (0.5 equivalents) or a peroxide (TBHP or H_2O_2) for different reaction times and temperatures were unsuccessful and led to either the recovery of **1** unchanged or (in the case of **3c**) only a very small crop of crystals with the oxo-bridged dimeric structure. Complex **5** is very soluble in polar aprotic solvents because of the presence of the Ph_3SiO groups, and crystals suitable for X-ray diffraction were readily obtained by slow evaporation of a saturated solution of the complex in CH_2Cl_2.

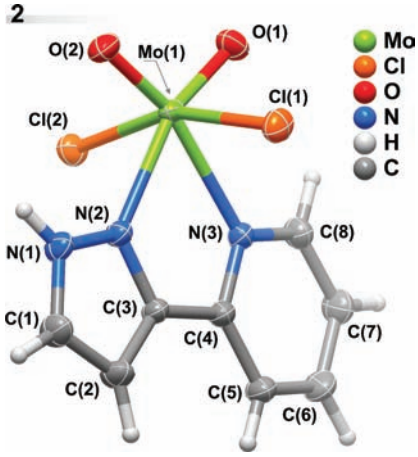

Figure 1. Schematic representation of the $[MoO_2Cl_2(PzPy)]$ molecular unit present in compound **2** showing all non-hydrogen atoms as thermal ellipsoids drawn at the 50% probability level and hydrogen atoms as small spheres with arbitrary radii. The atomic labeling scheme for all non-hydrogen atoms is provided. Selected bond lengths and angles describing the distorted octahedral $\{MoN_2O_4\}$ coordination environment of Mo^{VI} are listed in the Supporting Information, Table S1.

Crystal Structure Descriptions. Structure of $[MoO_2Cl_2(PzPy)]\cdot PzPyHCl$ (2). Compound **2** is a co-crystal composed of a discrete $[MoO_2Cl_2(PzPy)]$ complex (Figure 1) and a 2-[3(5)-pyrazolyl]pyridinium chloride salt. A search in the literature and in the Cambridge Structural Database (CSD, Version 5.31, November 2009) reveals that complexes of the type $[MoO_2X_2(L)_n]$, where L is one or

(24) Poulton, J. T.; Sigalas, M. P.; Folting, K.; Streib, W. E.; Eisenstein, O.; Caulton, K. G. *Inorg. Chem.* **1994**, *33*, 1476–1485.

(25) (a) Bingham, A. L.; Drake, J. E.; Hursthouse, M. B.; Light, M. E.; Kumar, R.; Ratnani, R. *Polyhedron* **2006**, *25*, 3238–3244. (b) Kühn, F. E.; Herdtweck, E.; Haider, J. J.; Herrmann, W. A.; Gonçalves, I. S.; Lopes, A. D.; Romão, C. C. *J. Organomet. Chem.* **1999**, *583*, 3–10. (c) Arzoumanian, H.; Agrifoglio, G.; Krentzien, H.; Capparelli, M. *J. Chem. Soc., Chem. Commun.* **1995**, 655–656. (d) Sens, I.; Stenger, H.; Muller, U.; Dehnicke, K. *Z. Anorg. Allg. Chem.* **1992**, *610*, 117–120. (e) Gupta, S.; Pal, S.; Barik, A. K.; Roy, S.; Hazra, A.; Mandal, T. N.; Butcher, R. J.; Kar, S. K. *Polyhedron* **2009**, *28*, 711–720. (f) Arzoumanian, H.; Bakhtchadjian, R.; Agrifoglio, G.; Atencio, R.; Briceno, A. *Transition Met. Chem.* **2008**, *33*, 941–951. (g) Baird, D. M.; Yang, F. L.; Kavanaugh, D. J.; Finness, G.; Dunbar, K. R. *Polyhedron* **1996**, *15*, 2597–2606. (h) Lachgar, A.; Farrall, P.; Mayer, J. M. *Polyhedron* **1993**, *12*, 2603–2609. (i) Dreisch, K.; Andersson, C.; Stalhandske, C. *Polyhedron* **1993**, *12*, 303–311. (j) Viossat, B.; Rodier, N. *Acta Crystallogr., Sect. C: Cryst. Struct. Commun.* **1979**, *35*, 2715–2718.

more N-containing ligand(s) and X is a halo ligand, are common.[4c,e,g,h,25] Nevertheless, to the best of our knowledge, **2** constitutes the first example of a fully characterized compound in which the desired chemical entity (the Mo^{VI}-containing complex) is embedded inside the supramolecular matrix of a hydrogen-bonded salt.

The structure contains a crystallographically independent Mo^{VI} center which is bound to two terminal oxo groups [Mo=O 1.6959(12) and 1.6972(12) Å], one *N*,*N*-chelated PzPy [Mo−N 2.2824(12) and 2.3492(13) Å; N−Mo−N bite angle 68.82(4)°] and two axially coordinated Cl atoms [Mo−Cl 2.3679(4) and 2.3784(4) Å]. The overall coordination sphere, $\{MoCl_2N_2O_2\}$, resembles a highly distorted octahedron for which the *cis* and *trans* internal octahedral angles range from 68.82(4) to 107.12(6)°, and from 160.276(15) to 161.17(6)°, respectively (Supporting Information, Table S1). This coordination environment closely resembles those of the aforementioned related structures described in the literature, in which the equatorial plane of the octahedron is composed of the oxo groups and the organic ligand; the *trans* ∠(Cl−Mo−Cl) angles range from about 157 to 163°.[4c,e,g,25e−25h,25j] One exception is the compound described by Dreisch and co-workers, $[MoO_2Cl_2(tmen)]$ (where tmen stands for *N*,*N*,*N*′,*N*′-tetramethylethylenediamine), in which all pairs of donor atoms are instead occupying *cis* positions within the coordination octahedron; the ∠(Cl−Mo−Cl) angle for this structure is about 87.5°.[25i]

The Mo^{VI} complex is directly involved in hydrogen bonding interactions with the charged species of the supramolecular salt (not shown): the N−H group of the coordinated PzPy donates its hydrogen to the charge-balancing chloride anion which, in turn, also receives a hydrogen from the protonated pyridinium ring of the 2-[3(5)-pyrazolyl]-pyridinium salt [even though the N−H···Cl distances are relatively long (>3 Å) the interactions approach linearity with angles >160°, see Supporting Information, Table S2]. The supramolecular structure is expanded by a $R_2^2(6)$ graph set motif[26] involving adjacent pyrazolyl rings and strong $\pi-\pi$ stacking interactions among spatially close PzPyH moieties.

Structures of $[Mo_2O_4(\mu_2\text{-}O)Cl_2(PzPy)_2]\cdot CH_3CN$ (3a), $[Mo_2O_4(\mu_2\text{-}O)Cl_2(PzPy)_2]$ (3b) and $[Mo_2O_4(\mu_2\text{-}O)Cl_2(PzPy)_2]\cdot 2THF$ (3c). This family of compounds comprises three distinct crystal structures of the binuclear $[Mo_2O_4(\mu_2\text{-}O)Cl_2(PzPy)_2]$ complex: two solvates with acetonitrile and THF, and a solvent-free structure. In the following paragraphs more emphasis will be given to the solvent-free structure and to that isolated with acetonitrile (Figure 2). Since our description of the structural features and properties of the dimeric complex $[Mo_2O_4(\mu_2\text{-}O)Cl_2(pzH)_4]$,[7] which joined that found by Atovmyan and co-workers in the early 1970s, $[Mo_2O_4(\mu_2\text{-}O)Cl_2(DMF)_4]$,[27] only one other related structure has been described containing two bidentate pyrazolyl-pyrimidine ligands.[25e] Zhang and co-workers recently described the hydrothermal synthesis of a higher nuclearity Mo^{6+} cluster (namely, tetranuclear $[Mo_4O_8(\mu_2\text{-}O)_4(PzPy)_4]$).[28]

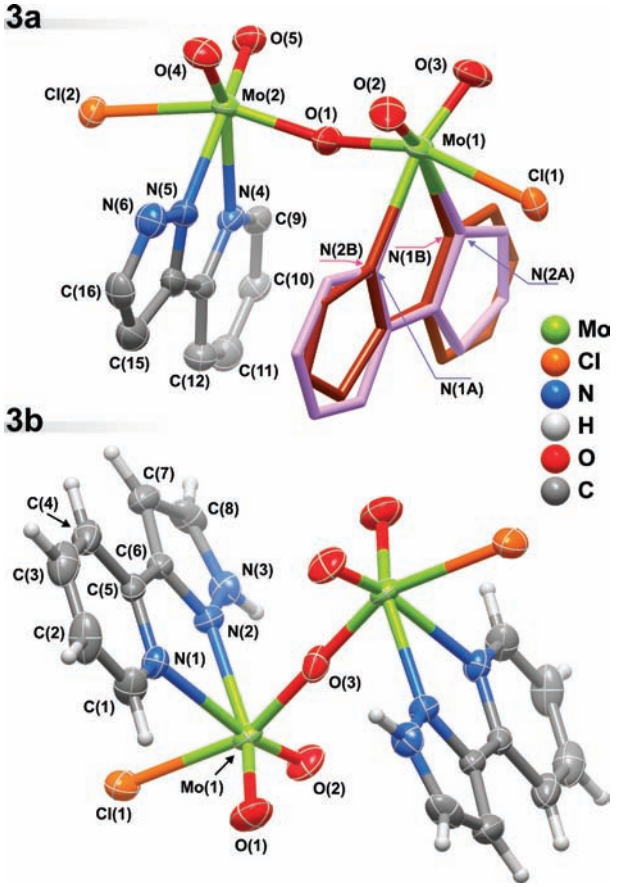

Figure 2. Schematic representations of the $[Mo_2O_4(\mu_2\text{-}O)Cl_2(PzPy)_2]$ molecular units present in compounds **3a** and **3b** showing all non-hydrogen atoms as thermal ellipsoids drawn at the 50% probability level and hydrogen atoms as small spheres with arbitrary radii. The atomic labeling scheme for selected non-hydrogen atoms is provided. The two superimposed crystallographic positions for the coordinated 2-[3(5)-pyrazolyl]pyridine in **3a** are represented in stick mode (in brown and violet). Selected bond lengths and angles describing the distorted octahedral $\{MoClN_2O_3\}$ coordination environments of Mo^{VI} are listed in the Supporting Information, Tables S3 and S5.

Each of the Mo^{VI} centers in complexes **3a**−**3c** are coordinated to two terminal oxo groups [Mo=O ranging from 1.6925(19) to 1.716(5) Å], one μ_2-bridging oxygen [Mo−O ranging from 1.8665(2) to 1.902(4) Å], one *N*,*N*-chelated PzPy ligand [Mo−N ranging from 2.299(2) to 2.364(2) Å; ∠(N−Mo−N) in the range of 68.34(19)-69.9(5)°], and one *exo*-coordinated Cl atom [Mo−Cl ranging from 2.4080(8) to 2.4449(18) Å]. The coordination environments resemble highly distorted octahedra, $\{MoClN_2O_3\}$, whose geometrical features agree relatively well with those found for the related compounds mentioned above.[7,25e,27]

In both the solvent-free (**3b**) structure and that with THF (**3c**), the $[Mo_2O_4(\mu_2\text{-}O)Cl_2(PzPy)_2]$ complex is centrosymmetric with the central μ_2-bridging oxygen being located at an inversion center, ultimately imposing Mo···Mo intermetallic separations of 3.7401(5) and 3.7330(3) Å, respectively. The analogous distance for the non-centrosymmetric

(26) Bernstein, J.; Davis, R. E.; Shimoni, L.; Chang, N. L. *Angew. Chem., Int. Ed. Engl.* **1995**, *34*, 1555–1573.

(27) Atovmyan, L. O.; Sokolova, Y. A.; Tkachev, V. V. *Doklady Akademii Nauk SSSR* **1970**, *195*, 1355–1356.

(28) Li, D.; Liu, Y.; Wei, P.; Hu, B.; Zhang, X. *Acta Crystallogr., Sect. E: Struct. Rep. Online* **2009**, *65*, m1074.

complex of **3a** is comparatively smaller [3.6900(11) Å] because of the "kink" angle associated with the bridge. Indeed, while in the centrosymmetric complexes the μ_2-bridge is completely linear, in **3a** it subtends an angle of 156.3(3)°, which promotes a shorter intermetallic distance. The complex described by Gupta et al. is also non-centrosymmetric, with the corresponding "kink" angle [148.87(14)°] and intermetallic distance (ca. 3.64 Å) agreeing well with those found for **3a**.[25e]

The complexes in **3a** and **3b**/**3c** differ concerning the mutual rotation of each individual $\{MoClN_2O_3\}$ octahedron. One would expect the organic moieties in these complexes to be positioned as far apart as possible to reduce the steric pressure on the complex. However, while this is the case in the latter structures, which have the *N*, *N*-chelated PzPy molecules located on opposite sides of the vector running through Cl→μ_2-O→Cl, in the former structure the organic ligands are located on the same side. Similarly, in the structure reported by Gupta et al.,[25e] the two pyrazolyl-pyrimidine ligands are approximately positioned on the same side of the Cl→μ_2-O→Cl vector (they are, in fact, slightly mutually rotated because of the presence of the methyl substituents on the aromatic rings). In the latter structure and in **3a** the organic moieties are disordered over two distinct positions (Figure 2). Because the distance between the average planes of the coordinated PzPy ligands in **3a** is larger than about 4 Å, we can exclude the existence of $\pi-\pi$ stacking interactions between neighboring coordinated moieties.

The crystal packing of **3a**−**3c** is strongly mediated by several hydrogen bonding interactions, which differ significantly among the members of the series. In the solvate structure **3c** (with THF) the coordinated PzPy moiety donates its hydrogen atom to a neighboring solvent molecule (Supporting Information, Table S8), with the close packing between adjacent complexes being essentially mediated by several cooperative, but weak, C−H···O interactions. Comparatively, the solvate **3a** is richer in terms of supramolecular contacts, with several strong and highly directional N−H···O and N−H···Cl hydrogen bonding interactions connecting adjacent molecular complexes (Supporting Information, Table S4). In this structure the encapsulated solvent molecule is solely involved in weak interactions with the hydrogen-bonded network formed by the complexes. In **3b** adjacent complexes are engaged in strong N−H···O hydrogen bonding interactions (Supporting Information, Table S6) forming an $R_2^2(10)$ graph set motif,[26] which is at the genesis of a one-dimensional supramolecular chain. Connections between neighboring chains are ensured by strong offset $\pi-\pi$ stacking interactions.

Structure of $[MoO(O_2)_2Cl(PzPyH)]$ (4). The asymmetric unit of **4** is composed of an anionic mononuclear Mo^{VI} complex, $[MoO(O_2)_2Cl]^-$, and a charge-balancing

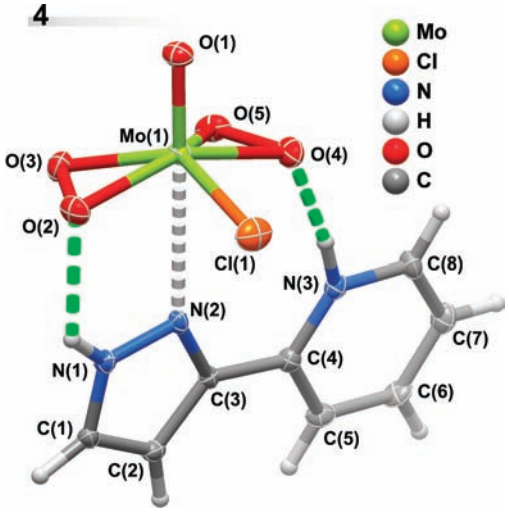

Figure 3. Schematic representation of the $[MoO(O_2)_2Cl(PzPyH)]$ molecular unit present in compound **4** showing all non-hydrogen atoms as thermal ellipsoids drawn at the 50% probability level and hydrogen atoms as small spheres with arbitrary radii. The atomic labeling scheme for all non-hydrogen atoms is provided. Selected bond lengths and angles describing the distorted tetrahedral coordination environment of Mo^{VI} and geometrical details on the hydrogen bonding interactions (dashed green lines) are listed in the Supporting Information, Tables S9 and S10.

2-[3(5)-pyrazolyl]pyridinium cation (Figure 3). Even though discrete mononuclear complexes having $MoO(O_2)_2$[4i,29] or $MoO(O_2)X$[30] cores (where X is a halogen) are relatively common, the anionic moiety found in **4** is truly unique because it constitutes, as far as we know, the first example of an oxodiperoxomolybdenum(VI) moiety coordinated to a halogen and further interacting with an organic ligand.

The crystallographically independent Mo^{VI} center in **4** is directly bound to two peroxo groups [Mo−O bonds ranging from 1.931(4) to 1.961(4) Å, see the Supporting Information, Table S9], one terminal oxo moiety [Mo=O 1.671(4) Å] and a Cl atom [Mo−Cl 2.3710(18) Å], with the coordination environment, $\{MoClO_5\}$, closely resembling a highly distorted tetrahedron if the center of gravity of each peroxo group is considered as the vertex of the polyhedron. In this simplification the internal tetrahedral angles range from about 100.1 to 129.6°.

As mentioned above, the most striking feature of the structure resides in the interaction of the PzPyH cation with the anionic moiety (Figure 3). The direct interaction of N(2) of the pyrazolyl group with the Mo^{VI} center (Mo···N ca. 2.82 Å) is strengthened by the existence of two peripheral and strong N−H···O hydrogen bonding interactions involving the N−H moieties and the peroxo groups (see the Supporting Information, Table S10). The N−H group of the pyrazolyl ring establishes a further connection (via hydrogen bonding) with a symmetry-related anionic complex, leading

(29) (a) Sensato, F. R.; Cass, Q. B.; Longo, E.; Zukerman-Schpector, J.; Custodio, R.; Andrés, J.; Hernandes, M. Z.; Longo, R. L. *Inorg. Chem.* **2001**, *40*, 6022–6025. (b) Piquemal, J.-Y.; Halut, S.; Brégeault, J.-M. *Angew. Chem., Int. Ed.* **1998**, *37*, 1146–1149. (c) Djordjevic, C.; Vuletic, N.; Jacobs, B. A.; Lee-Renslo, M.; Sinn, E. *Inorg. Chem.* **1997**, *36*, 1798–1805. (d) Thiel, W. R.; Priermeier, T.; Bog, T. *J. Chem. Soc., Chem. Commun.* **1995**, 1871–1872. (e) Thiel, W. R.; Priermeier, T. *Angew. Chem., Int. Ed. Engl.* **1995**, *34*, 1737–1738. (f) Winter, W.; Mark, C.; Schurig, V. *Inorg. Chem.* **1980**, *19*, 2045–2048. (g) Jacobson, S. E.; Tang, R.; Mares, F. *Inorg. Chem.* **1978**, *17*, 3055–3063.

(30) (a) Vrubel, H.; Horner, M.; Crespan, E. D.; Nakagaki, S.; Nunes, F. S. *Z. Anorg. Allg. Chem.* **2008**, *634*, 1839–1841. (b) Fronczek, F. R.; Luck, R. L.; Wang, G. *Inorg. Chem. Commun.* **2002**, *5*, 384–387. (c) Galakhov, M. V.; Gómez-Sal, P.; Pedraz, T.; Pellinghelli, M. A.; Royo, P.; Tiripicchio, A.; de Miguel, A. V. *J. Organomet. Chem.* **1999**, *579*, 190–197. (d) Chakraborty, D.; Bhattacharjee, M.; Krätzner, R.; Siefken, R.; Roesky, H. W.; Usón, I.; Schmidt, H.-G. *Organometallics* **1999**, *18*, 106–108. (e) Chaumette, P.; Mimoun, H.; Saussine, L.; Fischer, J.; Mitschler, A. *J. Organomet. Chem.* **1983**, *250*, 291–310. (f) Edwards, A. J.; Slim, D. R.; Guerchais, J. E.; Kergoat, R. *J. Chem. Soc., Dalton Trans.* **1977**, 1966–1968.

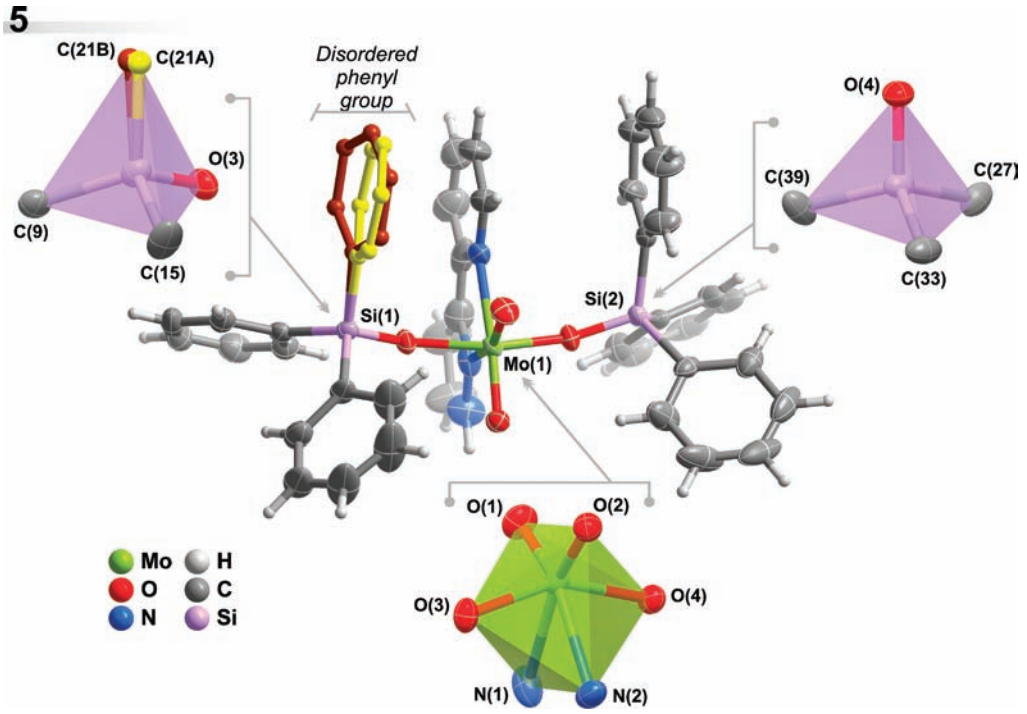

Figure 4. Schematic representation of the $[MoO_2(OSiPh_3)_2(PzPy)]$ molecular unit in complex **5**, showing all non-hydrogen atoms as thermal ellipsoids drawn at the 50% probability level, hydrogen atoms as small spheres with arbitrary radii, and the two crystallographic positions of the disordered phenyl group of $OSiPh_3$ in ball-and-stick mode (hydrogen atoms have been omitted for clarity; rates of occupancy are 54.8(6)% for the groups drawn in yellow and 45.2(6)% for the groups drawn in brown). Selected bond lengths and angles are listed in the Supporting Information, Table S11.

to the formation of an $R_2^2(4)$ graph set motif (not shown),[26] which promotes the assembly of a supramolecular arrangement of dimers in the crystal structure of **4**.

$[MoO_2(OSiPh_3)_2(PzPy)]$ (5). Molybdenum complexes with triphenylsiloxy groups in the first coordination sphere are not very common.[25f,31] The reported complexes that are most closely related to that in **5** are $[MoO_2(OSiPh_3)_2$-(4,4′-di-*tert*-butyl-2,2′-bipy],[25f] $[MoO_2(OSiPh_3)_2(phen)]$, and $[MoO_2(OSiPh_3)_2(py)_2]$ (where phen = 1,10-phenanthroline and py = pyridine).[31d]

As found for **2**, the asymmetric unit in **5** contains a single Mo^{VI} center exhibiting a highly distorted $\{MoN_2O_4\}$ octahedral coordination geometry in which the equatorial plane is composed of two terminal oxo groups [Mo=O 1.696(3) and 1.701(3) Å] and an *N*,*N*-chelating 2-[3(5)-pyrazolyl]pyridine [Mo−N 2.353(4) and 2.407(4) Å; N−Mo−N bite angle 67.08(17)°]. The axial positions of the coordination polyhedron are occupied by two triphenylsiloxy moieties with the Mo−O distances ranging from 1.923(3) to 1.937(3) Å (Figure 4). When compared with the geometrical features of the $\{MoCl_2N_2O_2\}$ coordination sphere in **2**, in **5** the Mo−N bond lengths are longer (see the Supporting Information, Tables S1 and S11). This difference can be attributed to the presence of the triphenylsiloxy moieties which, on the one hand, weaken the Mo−N interactions because the Mo−O bond distances are considerably shorter than the Mo−Cl ones (in **2**) and, on the other, impose a greater steric pressure near the Mo^{VI} center (compared with the chlorido ligands in **2**), which promote a reduction in the binding strength of PzPy (as also revealed by the decrease in the corresponding N−Mo−N bite angle). These considerations are in line with the conclusions drawn from a comparison of the ^{1}H NMR (see above) and IR/Raman (see below) data for **1** and **5**. It is also worth noting that the O−Mo−O angle observed in **5** [151.71(14)°] is smaller than the analogous Cl−Mo−Cl angle in **2** [160.276(15)°], further supporting the enhanced steric pressure around the metal center in **5** which promotes a higher polyhedral distortion. Nevertheless, this registered O−Mo−O angle agrees with those observed in related structures.[25f,31d]

The crystal packing in **5** is essentially mediated by the need to effectively fill the available space, with several C−H···π interactions (not represented) promoting some structural robustness. Remarkably, because of the large molecular size of the triphenylsiloxy moieties, which induces a greater distance between neighboring complexes, the N−H moiety of the coordinated PzPy ligand is not engaged in hydrogen bonding interactions, in contrast with that found for the other complexes.

Vibrational Spectroscopy and DFT Calculations. Table 2 lists the most characteristic and representative metal−ligand vibrations for the molybdenum complexes **1**, **3a**, **4**, and **5**. Overall, there is a good qualitative agreement between experimental and calculated values, considering that the experimental spectra are for the condensed phase while the calculations consider only the isolated molecule. The bands arising from Mo=O vibrations are intense and characteristic in the IR and Raman spectra of *cis*-dioxo complexes, with two Mo=O stretching modes (νMo=O) and a deformation mode

(31) (a) Wang, J. J.; Holm, R. H. *Inorg. Chem.* **2007**, *46*, 11156–11164. (b) Ma, X. L.; Yang, Z.; Schulzke, C.; Ringe, A.; Magull, J. *Z. Anorg. Allg. Chem.* **2007**, *633*, 1320–1322. (c) Lim, B. S.; Willer, M. W.; Miao, M. M.; Holm, R. H. *J. Am. Chem. Soc.* **2001**, *123*, 8343–8349. (d) Thapper, A.; Donahue, J. P.; Musgrave, K. B.; Willer, M. W.; Nordlander, E.; Hedman, B.; Hodgson, K. O.; Holm, R. H. *Inorg. Chem.* **1999**, *38*, 4104–4114. (e) Huang, M. D.; Dekock, C. W. *Inorg. Chem.* **1993**, *32*, 2287–2291. (f) Klemperer, W. G.; Mainz, V. V.; Wang, R. C.; Shum, W. *Inorg. Chem.* **1985**, *24*, 1968–1970.

Table 2. Selected Raman and IR Bands (cm^{-1}) for Complexes **1**, **3a**, **4**, and **5**,[a] and Calculated (B3LYP) Values

complex	calcd[b]	IR	Raman	assignment
1	932	940s	937vs	νMo=O_{sym}
	918	906vs	909s	νMo=O_{asym}
	337	395w	397 m	γMoO_2
	308	345 m		νMo−Cl_{asym}
	276		222 m	νMo−Cl_{sym}
	151		171w	νMo−N_{sym}
	137			νMo−N_{asym}
3a	924	942s	936 m	νMo=O_{sym}
	897	906vs	907w	νMo=O_{asym}
	805	773sh[c]		ν(Mo−O−Mo)$_{asym}$
	352	448w		δ(Mo−O−Mo)
	337	394w	395 m	γMoO_2
	326	371w		ν(Mo−O−Mo)$_{sym}$
	272	335 m		νMo−Cl_{asym}
	260		222 m	νMo−Cl_{sym}
	147		166vw	νMo−N_{sym}
	136			νMo−N_{asym}
4	980	985s	992s	νMo=O
	873	874sh	877s	ν(O−O)$_{asym}$
	867	858s		ν(O−O)$_{sym}$
	563	580s	584 m	ν(Mo−O)$_{peroxo}$
	535	540 m	543s	ν(Mo−O)$_{peroxo}$
	491	504w	504w	ν(Mo−O)$_{peroxo}$
	456	454 m	457w	ν(Mo−O)$_{peroxo}$
	316	349 m	348w	νMo−Cl
	180		184 m	βMo−Cl
5	946	925vs[d]	925 m	νMo=O_{sym}
	922	904sh[d]	904 m	νMo=O_{asym}
	455	462w		νMo−O_{asym}
	439	430w	430vw	νMo−O_{sym}
	341	382w	383 m	γMoO_2
	192	278 m	283sh	νMo−N_{sym}
	127		196w	νMo−N_{asym}

[a] Abbreviations: sh = shoulder, vs = very strong, vw = very weak, m = medium, w = weak. [b] Scaled values (scale factor = 0.961). [c] Overlap with strong γCH bands of PzPy ligand. [d] Overlap with strong νO−Si bands.

(γMoO_2) being expected.[32] In the IR spectra of **1** and **3a**, the pairs of intense bands at 906/940 cm^{-1} and 906/942 cm^{-1} are assigned to the asymmetric and symmetric stretching vibrations of the *cis*-$[MoO_2]^{2+}$ core (Figure 5). The weak band observed at 928 cm^{-1} is assigned to a PzPy ligand vibration. For complex **5**, the asymmetric Mo=O stretching band appears as a shoulder at 904 cm^{-1} on the strong νO−Si bands from the $MoO_2(OSiPh_3)_2$ fragment. Comparing the experimental νMo=O wavenumbers for complexes **1** and **5**, the higher values observed for the dichloro complex suggest that the Mo=O bonds are strengthened when the Mo−O (triphenylsiloxy) bonds are replaced by Mo−Cl bonds.[4c] This is consistent with the above discussion concerning the relative donor powers of Cl and Ph_3SiO in the two complexes since, if the donor power of the Cl groups in **1** is lower than that for the Ph_3SiO groups in **5**, one would expect more electron density to be shifted from the other ligands thereby strengthening the metal−ligand bonds.[33] Against this, the DFT calculations predict that the νMo−N_{sym} stretching mode should appear at higher wavenumber for **5** than for **1**, while the corresponding asymmetric mode should appear at lower wavenumber. However, these trends should be treated with caution since the calculations also gave νMo=O stretching frequencies that were higher for **5** than for **1**, which is the opposite of the observed trend. What is clear is that the

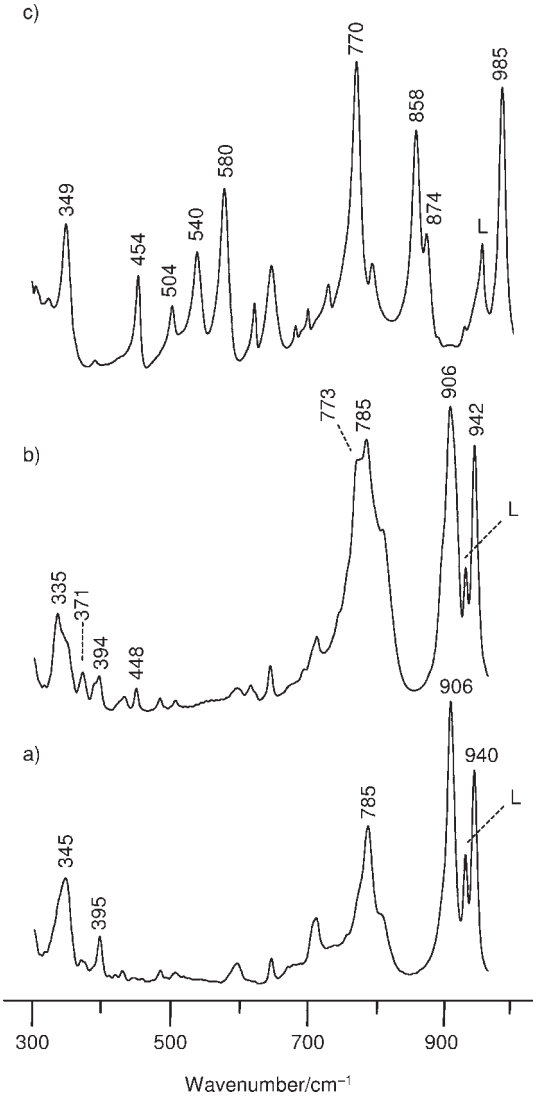

Figure 5. IR spectra in the region of 300−950 cm^{-1} for (a) the monomeric complex **1**, (b) the oxo-bridged dimer **3a**, and (c) the oxodiperoxo complex **4**. Ligand-centered bands are denoted by L.

strengths of the interactions within the equatorial MoO_2N_2 plane change on going from complexes **1** to **5**, in agreement with that previously reported for the analogous complexes bearing the ligand ethyl[3-(2-pyridyl)-1-pyrazolyl]acetate.[4e]

The presence of a binuclear complex in **3a** is indicated by the IR bands at 371, 448, and 773 cm^{-1}, which are not present in the spectrum of **1** (Figure 5). On the basis of the DFT calculations, the band at 371 cm^{-1} is assigned as the symmetric stretching mode, ν(Mo−O−Mo)$_{sym}$, while the band at 448 cm^{-1} is assigned to the out-of-plane deformation, δ(Mo−O−Mo). Although the band related with the asymmetric stretching mode, ν(Mo−O−Mo)$_{asym}$, is expected to be very strong in the IR, in agreement with previous studies,[34−36] it is only observed as a shoulder at 773 cm^{-1}, being almost obscured by the strong band at 785 cm^{-1} assigned to C−H out-of-plane bending modes

(32) Griffith, W. P. *J. Chem. Soc. A* **1969**, 211–218.
(33) Topich, J.; Bachert, J. O., III *Inorg. Chem.* **1992**, *31*, 511–515.
(34) Arzoumanian, H.; Bakhtchadjian, R.; Agrifoglio, G.; Krentzien, H.; Daran, J.-C. *Eur. J. Inorg. Chem.* **1999**, 2255–2259.
(35) Brito, J. A.; Gómez, M.; Muller, G.; Teruel, H.; Clinet, J.-C.; Duñach, E.; Maestro, M. A. *Eur. J. Inorg. Chem.* **2004**, 4278–4285.
(36) Monteiro, B.; Gago, S.; Neves, P.; Valente, A. A.; Gonçalves, I. S.; Pereira, C. C. L.; Silva, C. M.; Pillinger, M. *Catal. Lett.* **2009**, *129*, 350–357.

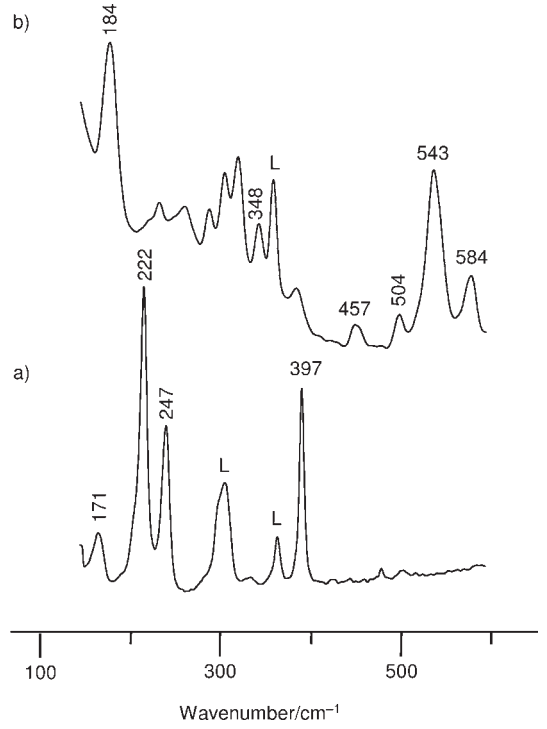

Figure 6. Raman spectra in the region of 100−600 cm^{-1} for (a) the monomeric complex **1** and (b) the oxodiperoxo complex **4**. Ligand-centered bands are denoted by L.

of the PzPy ligand. The latter band appears at the same frequency for complex **1** and 770 cm^{-1} for complex **4**. Neither bands for $\nu(Mo-O-Mo)_{sym/asym}$ nor $\delta(Mo-O-Mo)$ are observed in the Raman spectrum of **3a**.

The out-of-plane deformation mode, γMoO_2, occurs as a medium-intensity band at 397, 395, and 383 cm^{-1} in the Raman spectra of complexes **1** (Figure 6a), **3a**, and **5**, respectively. In the corresponding IR spectra only weak bands at 395 cm^{-1} (Figure 5a), 394 cm^{-1} (Figure 5b), and 382 cm^{-1} (Table 2) are observed. As expected for the monooxo-diperoxo complex **4**, this characteristic band of the *cis*-$[MoO_2]^{2+}$ group is not observed in the IR (Figure 5c) or Raman (Figure 6b) spectra, which supports the assignment in the spectra of **1**, **3a**, and **5**.

The vibrational Mo=O and O−O stretching modes for complex **4** appear as sharp and very strong bands. The IR spectrum (Figure 5c) shows the νMo=O band at 985 cm^{-1}, while two bands at 874 and 858 cm^{-1} are found for the asymmetric and symmetric ν(O−O) modes, respectively. Additionally, four bands assigned to the metal−peroxo stretching modes, $\nu(Mo-O)_{peroxo}$, appear in both the IR (580, 540, 504, 454 cm^{-1}, Figure 5c) and Raman (584, 543, 504, 457 cm^{-1}, Figure 6b) spectra. The relatively high νMo=O and low ν(O−O) wavenumbers (compared with the values typically reported for related compounds of the type $[MoO(O_2)_2(L)]$, where L is a neutral bidentate N, N-ligand[9,35,37]) are explained by the very distinct molecular structure of **4**, which comprises one Cl group *cis* to the oxo ligand, one very weakly coordinated pyrazole nitrogen in the axial position *trans* to the Mo=O bond, and hydrogen bonding interactions between the NH groups of the pyrazole/pyridinium rings and the peroxo ligands. As reported previously for complexes of the type $[MoO(O_2)_2(L')(L'')]$,[38] donor ligands *trans* to Mo=O reduce the Mo−O bond order (and hence the Mo=O stretching frequency) by donating electron density to the metal center. In **4** the weak coordination between the pyrazole nitrogen and the metal center will be compensated by more electron density being donated from the oxo group, resulting in a higher Mo−O bond order. The unlabeled bands in the Raman spectrum of **4** (Figure 6b) are tentatively assigned to out-of-plane $(Mo-O)_{peroxo}$ vibrations.

The DFT calculations predict that the νMo−Cl vibrations will occur in the 260−316 cm^{-1} range for complexes **1**, **3a**, and **4**. In the far-IR spectra of complexes **1** and **3a**, the experimental bands at 345 cm^{-1} (Figure 5a) and 335 cm^{-1} (Figure 5b) are assigned to $\nu Mo-Cl_{asym}$, while Raman bands of moderate intensity at 222 cm^{-1} (Figure 6a) are assigned to $\nu Mo-Cl_{sym}$. Additionally, a Mo−Cl deformation mode is predicted to occur at 180 cm^{-1} for complex **4**, lower than the 316 cm^{-1} predicted for the νMo−Cl mode. Thus, the bands at 349 cm^{-1} in the IR spectrum (Figure 5c) and 348 cm^{-1} in the Raman spectrum can be assigned to the νMo−Cl mode, while the βMo−Cl mode is assigned to a strong Raman band at 184 cm^{-1} (Figure 6b). Considering the νMo−N modes that arise from complexation of the PzPy ligand with the metal center, these are identified as weak bands in the Raman spectra of complexes **1**, **3a**, and **5**. The weak band at 171 cm^{-1} for complex **1** (Figure 6a) is assigned to $\nu Mo-N_{sym}$.

The assignment of the extra Raman band at 247 cm^{-1} for complex **1** (Figure 6a) is quite difficult and uncertain. However, considering that this band is absent from the Raman spectrum of the peroxo complex **4** (Figure 6b), a possible assignment is the in-plane deformation mode βMoO_2, which is predicted by DFT calculations to occur at 220 cm^{-1}.

A detailed analysis of the vibrational spectra of complexes **1**, **3a**, **4**, and **5**, and the corresponding free ligand and precursors, provides evidence for structural changes in the PzPy ligand upon complexation. Figure 7 demonstrates some of these changes for complex **5**. In the 1550−1650 cm^{-1} region of the Raman spectrum, the bands arising from the N−C−C−N fragment of the ligand, the C−C pyridine vibrations, and the C−N stretching ring vibrations shift to higher wavenumbers upon coordination to the Mo center, in agreement with previous results.[4e] Specifically, the bands of PzPy at 1565 cm^{-1} (PzPy-C−C inter-ring stretching mode), 1590 cm^{-1} (Py-C−N stretching mode), and 1597 cm^{-1} (Py-C−C stretching mode) are shifted to 1568, 1605, and 1609 cm^{-1}, respectively. A similar trend is observed for complexes **1** and **3a**. The band observed at 1590 cm^{-1} for complex **5** can be assigned to a vibration from the $MoO_2(OSiPh_3)_2$ fragment, and accordingly is not observed in the Raman spectra of complexes **1**, **3a**, and **4**.

The crystallographic studies of **4** provide evidence for the protonation of the pyridine nitrogen. The DFT

(37) Carreiro, E. P.; Yong-En, G.; Burke, A. J. *Inorg. Chim. Acta* **2006**, *359*, 1519–1523.

(38) Wahl, G.; Kleinhenz, D.; Schorm, A.; Sundermeyer, J.; Stowasser, R.; Rummey, C.; Bringmann, G.; Fickert, C.; Kiefer, W. *Chem.—Eur. J.* **1999**, *5*, 3237–3251.

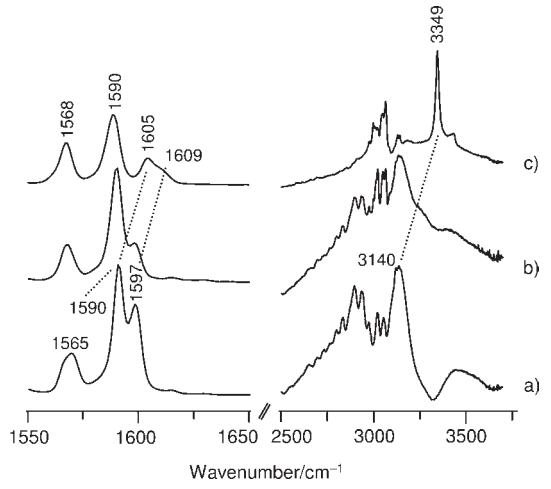

Figure 7. Comparison of the Raman (1550−1650 cm^{-1} region) and IR (2500−3700 cm^{-1} region) spectra of (a) the ligand PzPy, (b) the weighted sum of the spectra of the ligand and the precursor $MoO_2(OSiPh_3)_2$, and (c) the triphenylsiloxy complex **5**.

calculations predict that this protonation should shift the bands mentioned above to higher wavenumbers. Accordingly, the Raman bands are observed at 1570, 1610, and 1634 cm^{-1}.

The IR spectrum of complex **5** emphasizes another effect of ligand complexation, which is also observed for the other complexes. The band assigned to the stretching of the pyrazole N−H group shifts from around 3140 cm^{-1} for the free PzPy to 3349 cm^{-1} for **5**, 3287 cm^{-1} for **4**, 3252 cm^{-1} for **3a**, and 3258 cm^{-1} for **1**. These different shifts can be explained by the presence or otherwise of distinct intramolecular and/or intermolecular hydrogen bonds involving the moieties of each structure. In fact, the cleavage of the strong intermolecular N−H···N hydrogen bonding for the PzPy molecules (see ref 39 for the crystal structure of PzPy) as a result of geometrical restrictions imposed by complex formation promotes the shift to higher frequencies. As discussed above, the X-ray structural studies support the presence of hydrogen bonds involving the pyrazole N−H group for complexes **3a** and **4**, but not complex **5**. This explains the higher shift observed for **5** where the N−H group is considered to be free. For the other two complexes, the hydrogen bonds are expected to weaken the N−H bond and therefore lower the stretching frequency.

Cyclooctene Epoxidation. The catalytic performance of complexes **1** and **5** for olefin epoxidation was investigated using *cis*-cyclooctene (Cy) as a model substrate, TBHP (5.5 M in decane) as oxidant, a reaction temperature of 55 °C, and no additional co-solvent. A catalyst/substrate/oxidant molar ratio of 1:100:150 was used. In the absence of a catalyst Cy conversion at 24 h was 5%. Figure 8 shows the kinetic curves obtained for complexes **1** and **5**. The initial reaction rate is much higher for complex **1**, with conversions at 10 min being 32% for **1** and 4% for **5**. However, the kinetic curves tend to converge for longer reaction times, giving conversions at 6 h/24 h of about 66%/90% for both complexes (Table 3). 1,2-Epoxycyclooctane was the only reaction product observed. A similar relation

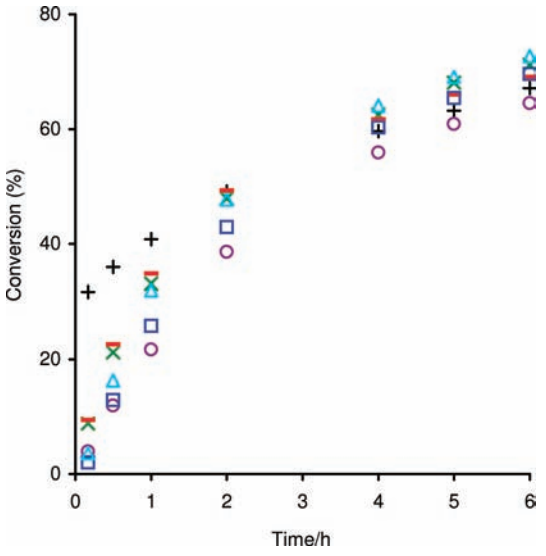

Figure 8. Cyclooctene epoxidation at 55 °C using TBHP and complex **1** (+), **1*** (×), **1**** (−), complex **5** (○), **5*** (□), and **5**** (△). **1*** and **5*** are the insoluble materials recovered after the catalytic runs using **1** and **5**, while **1**** and **5**** are the insoluble materials recovered after the catalytic runs using **1*** and **5***.

Table 3. Epoxidation of *cis*-Cyclooctene Using TBHP at 55 °C

	conversion at 6 h/24 h (%)		
precursor complex	run 1	run 2	run 3
1	67/90	71/93	69/91
5	65/90	70/93	73/96

between catalytic activities was reported previously for analogous chloro and triphenylsiloxy derivatives of dioxomolybdenum(VI) chelated with substituted pyrazolylpyridines, namely, 2-(1-butyl-3-pyrazolyl)pyridine and ethyl[3-(2-pyridyl)-1-pyrazolyl]acetate.[4e]

At 24 h the reaction mixtures for **1** and **5** consisted of a suspension containing an insoluble or very poorly soluble white solid, which was recovered by centrifugation as described in the Experimental Section, giving materials identified as **1*** and **5***. When a second 24 h catalytic run was performed using **1*** (without sampling), the amount of solid (hereafter referred to as **1****) recovered at the end of the reaction was about 90 wt % of that initially charged to the reaction vessel. Figure 8 shows the kinetic curves obtained for second and third runs carried out using **1***/**5*** and **1****/**5****; the solids recovered at the ends of the third runs are denoted as **1*****/**5*****. The curves for **5**, **5*** and **5**** are similar. The curves for **1*** and **1**** are practically identical, and very similar to those for **5**/**5***/**5****. Complex **1** shows a higher initial reaction rate, but after 2 h the curves converge.

The lower initial reaction rate observed for **1*** compared with **1** may be due to the presence of a fraction of dissolved active species in the first run with **1**. This was supported by the fact that a leaching test performed (as described in the Experimental Section) for complex **1** gave an increment in conversion between 1 and 6 h of 17%, compared with 26% when no solid was separated. The solution filtered off at 1 h was pale yellow, consistent with the presence of molybdenum(VI) complexes (see, for example, compounds **1**−**4** prepared in the present work, which are yellow). Attempts to characterize or isolate the

(39) Singh, K.; Long, J. R.; Stavropoulos, P. *J. Am. Chem. Soc.* **1997**, *119*, 2942–2943.

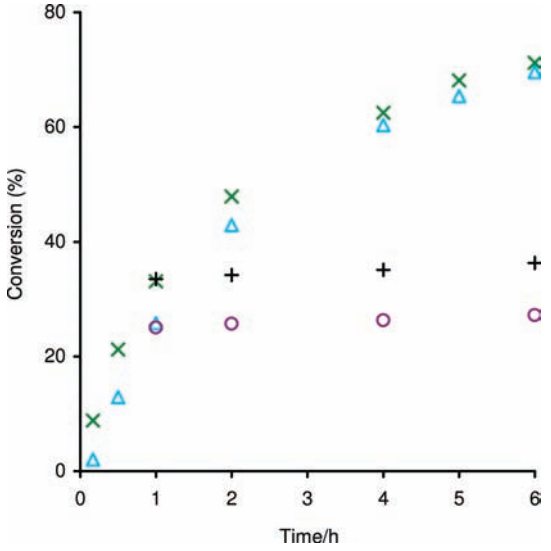

Figure 9. *cis*-Cyclooctene epoxidation at 55 °C using TBHP and **1*** (×, +) or **5*** (△,○). The reactions identified by × and △ are the same as run 2 for complexes **1** and **5**, respectively, while + and ○ correspond to the leaching tests with hot-filtration at 1 h reaction for **1*** and **5***.

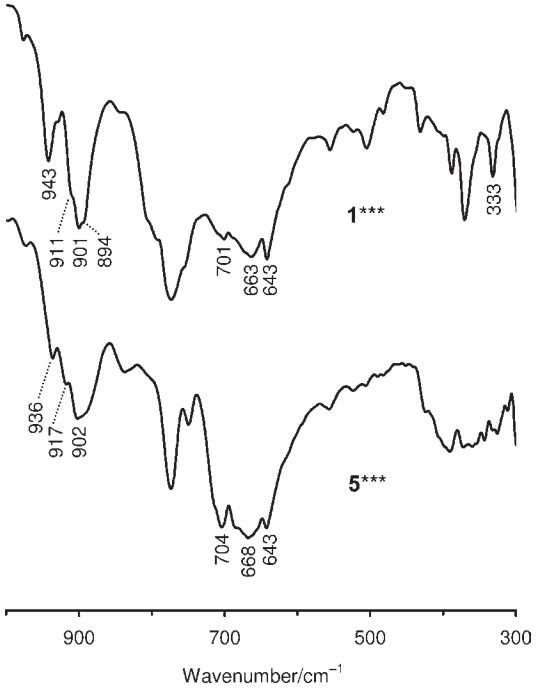

Figure 10. ATR FT-IR spectra in the region of 300−1000 cm^{-1} for the recovered solids **1***** and **5*****.

species in solution were unsuccessful, mainly because of the very low concentrations involved. Leaching tests were also performed for the white solids **1*** and **5*** to investigate the homo/heterogeneous nature of the catalytic reactions; the results are shown in Figure 9 and compared with the kinetic curves obtained for **1*** and **5*** (i.e., with no filtration step at 1 h). For **1*** and **5***, after separating the solid at 1 h, the reaction of Cy is negligible up to 6 h, suggesting that the catalytic reactions with **1*** and **5*** are essentially heterogeneous in nature. This is consistent with the apparent good recyclability of the two solids (cf. the kinetic curves for **1***/**1**** and **5***/**5****). In a separate catalytic run carried out using a lower amount of **1*** (0.7 g/L instead of 8.1 g/L), the conversions at 6 h/24 h (55%/79%) were lower than those obtained for the higher amount (71%/93%, Table 3).

In the case of complex **5**, triphenylsilanol (Ph_3SiOH) was detected in the reaction mixture by GC-MS, indicating that hydrolysis of the Mo−$OSiPh_3$ bonds took place because of the presence of water in the reaction mixture (from the TBHP solution, for example, which may contain up to 4% water). Hydrolysis of the Mo−Cl bonds in **1** would give HCl, which cannot be detected by GC-MS. ATR FT-IR spectra were measured for all of the recovered solids; the spectra for **1***** and **5***** are shown in Figure 10. The spectra for **5***, **5****, and **5***** were essentially identical, but very different from that for **5**. Thus, the complete loss of triphenylsiloxy groups was confirmed by the disappearance of the strong bands at 1115 and 508 cm^{-1}, which are attributed to νSi−O and X-sensitive Ph vibrations, respectively. The weak band at 462 cm^{-1} for **5** (νMo−O_{asym}) was also absent in the spectrum of **5***. Several new bands appeared for the recovered solid, including a well resolved shoulder at 936 cm^{-1}, and overlapping bands between 625 and 725 cm^{-1} with maxima at 643, 668, and 704 cm^{-1}. The shoulder at 936 cm^{-1} can be assigned to νMo=O, while the other bands are probably due to ν(Mo−O−Mo) and may indicate the formation of a molybdenum oxide cluster or polymer.

Comparing the spectra of **1** and **1***, there were several significant changes worth noting. In the range of 850−950 cm^{-1} the pair of intense νMo=O bands at 906/940 cm^{-1} were replaced by bands at 901 and 943 cm^{-1}, with shoulders at about 894 and 911 cm^{-1}. The medium intensity νMo−Cl band at 345 cm^{-1} for **1** was replaced by a weaker band at 333 cm^{-1}, which matches the νMo−Cl wavenumber observed for the oxo-bridged dimer **3a**. On the other hand, in line with that observed for **5***, several overlapping absorption bands appeared in the range of 625−725 cm^{-1}, which gained intensity on going from **1*** to **1***** and have maxima (643, 663, and 701 cm^{-1}) in agreement with those observed for **5*** (Figure 10). Thus, a similar type of molybdenum oxide cluster or polymer seems to be forming. If the 333 cm^{-1} band is due to νMo−Cl, it may indicate that the hydrolysis of the Mo−Cl bonds is slower than that observed for Mo−$OSiPh_3$, resulting in the formation of dimeric and/or oligomeric products with some Mo−Cl bonds still intact. The low solubility of **1** compared with **5** may be a contributing factor to these differences.

The spectra of all of the recovered solids contained several medium/weak bands in the range of 1000−1650 cm^{-1}, which are assigned to ligand-centered vibrations. In particular, the presence of the bands at 1571 and 1611 cm^{-1} is consistent with a bidentate coordination of the ligand as in complexes **1** and **5**. The absence of an additional strong band close to 1630 cm^{-1} (as seen for compounds **2** and **4**) probably means that the pyridine nitrogen was not protonated. Finally, the spectra provided no characteristic bands for peroxo species, ruling out the presence of complexes of the type **4** or oxodiperoxo species such as [$MoO(O_2)_2$(PzPy)].

The solid **5*** was further characterized by elemental analysis, SEM-EDS, and powder XRD. Elemental analysis gave 29.30% carbon, 2.65% hydrogen, 12.25% nitrogen, and 35.0% molybdenum. This gives a C/N

molar ratio of 2.8, which is close to the expected value of 2.7 for the PzPy ligand, and a Mo/ligand molar ratio of 1.2. The SEM images of **5** and **5*** showed irregular morphologies and particles sizes essentially in the range of 0.1−1 μm (Supporting Information, Figure S1). Employing an elemental mapping technique, spatial elemental profiles were generated for Si and/or Mo (Supporting Information, Figure S1). The profiles for **5** revealed a homogeneous distribution of Mo and Si with a Si/Mo ratio in the range of 1.7−2.4, which is in reasonable agreement with the expected value of 2. For the recovered solid **5*** the EDS mapping microimages revealed an even distribution of molybdenum and no silicon was detected, which is consistent with the ATR FT-IR data discussed above. Powder XRD data are given in Supporting Information, Figure S2. The pattern for **5** was in reasonable agreement with the simulated pattern calculated from the crystal structure of **5** determined in the present work. By contrast, the pattern for **5*** was very different, showing several sharp and intense reflections superimposed on some very broad peaks. All of the well-defined reflections can be assigned to the tetranuclear complex mentioned above, $[Mo_4O_8(\mu_2\text{-}O)_4(PzPy)_4]$, as proven by a comparison with the simulated pattern calculated from the crystal structure described by Zhang and co-workers.[28] The elemental analysis results for **5*** deviate somewhat from the calculated values for the tetranuclear complex ($C_{32}H_{28}Mo_4N_{12}O_{12}$: C, 33.24; H, 2.44; N, 14.54; Mo, 33.2%), which may be linked with the presence of the amorphous phase evidenced by the powder XRD data.

Conclusions

The complex $[MoO_2Cl_2(PzPy)]$ (**1**) can be readily prepared in high yields by the treatment of the solvent adduct $[MoO_2Cl_2(THF)_2]$ with the pyrazolylpyridine ligand. Attempts to obtain single crystals of **1** are hampered by the low solubility of the complex; the necessarily long crystallization times resulted in partial degradation, giving structures containing either mononuclear $[MoO_2Cl_2(PzPy)]$ co-crystallized with PzPyHCl, binuclear $[Mo_2O_4(\mu_2\text{-}O)Cl_2(PzPy)_2]$, or the oxodiperoxomolybdenum(VI) complex $[MoO(O_2)_2Cl(PzPyH)]$. The nature of the solvent strongly influences the outcome of the crystallization. The tendency to form oxo-bridged dimers of the type $[Mo_2O_4(\mu_2\text{-}O)Cl_2(L)_n]$ is in agreement with previous studies with complexes of the type $[MoO_2Cl_2(L)_n]$ containing either *N*,*N*-dialkylamide or substituted 2,2′-bipyridine ligands, and has implications for the use of the mononuclear complex as a catalyst for the epoxidation of olefins. When compared with $[MoO_2X_2(L)_n]$ complexes already described, complexes **1** and $[MoO_2(OSiPh_3)_2(PzPy)]$ (**5**) are medium active dioxomolybdenum(VI) catalysts for the epoxidation of cyclooctene (used as a model substrate). Under the reaction conditions used, complex **5** loses the triphenylsiloxy groups to give the tetranuclear complex, $[Mo_4O_8(\mu_2\text{-}O)_4(PzPy)_4]$. Starting from complex **1**, a similar type of molybdenum oxide cluster or polymer seems to form during three consecutive reaction runs, and we may speculate that the formation of an oxo-bridged dimer is the first step. Interestingly, the recovered molybdenum-containing materials can be used as stable, recyclable heterogeneous catalysts for the epoxidation reaction, and therefore warrant further structural characterization and investigation as catalysts in target epoxidation reactions of industrial interest. These studies are currently under way in our laboratories.

Acknowledgment. We are grateful to the Fundação para a Ciência e a Tecnologia (FCT), the Programa Operacional Ciência e Inovação (POCI) 2010, Orçamento do Estado (OE) and Fundo Europeu de Desenvolvimento Regional (FEDER) for funding (Project PTDC/QUI/71198/2006). The FCT is acknowledged for a Ph.D. grant to A.C.C. and for the financial support towards the purchase of the Bruker APEX II single-crystal diffractometer.

Supporting Information Available: Crystallographic data for compounds **2**, **3a**−**3c**, **4**, and **5** (CIFs and Tables S1−11 listing selected bond lengths and angles for the Mo^{VI} coordination environments and hydrogen bonding geometries), and SEM images, elemental maps, and powder XRD patterns for **5** and **5*** (Figures S1 and S2). This material is available free of charge via the Internet at http://pubs.acs.org.